



# HUSKYWORKS

EDUCATE AND COMPETE



# UW-21 DRAGONFLY

# Contents

<b>1</b>	<b>Executive Summary</b>	<b>4</b>
<b>2</b>	<b>Management Summary</b>	<b>5</b>
2.1	Team Organization . . . . .	5
2.2	Milestone Chart . . . . .	6
<b>3</b>	<b>Conceptual Design</b>	<b>6</b>
3.1	Mission Requirements and Constraints . . . . .	6
3.2	Design Parameters and Constraints . . . . .	9
3.3	Configuration Selection . . . . .	13
3.4	Final Conceptual Design Configuration . . . . .	16
<b>4</b>	<b>Preliminary Design</b>	<b>16</b>
4.1	Design Methodology . . . . .	16
4.2	Design Trade Studies . . . . .	17
4.3	Aerodynamics . . . . .	20
4.4	Aircraft Stability Analysis . . . . .	25
4.5	Predicted Aircraft Mission Performance . . . . .	27
<b>5</b>	<b>Detailed Design</b>	<b>28</b>
5.1	Dimensional Parameters . . . . .	28
5.2	Structure Characteristics and Capabilities . . . . .	28
5.3	Subsystem Design . . . . .	29
5.4	Weight and Balance . . . . .	36
5.5	Predicted Aircraft Flight and Mission Performance . . . . .	37
5.6	Drawing Package . . . . .	37
<b>6</b>	<b>Manufacturing Plan</b>	<b>42</b>
6.1	Manufacturing Processes Investigated . . . . .	42
6.2	Processes Selected: Aerodynamic Prototype . . . . .	43
6.3	Processes Selected: Competition Aircraft . . . . .	45
6.4	Manufacturing Schedule . . . . .	48
<b>7</b>	<b>Test Plan</b>	<b>49</b>
7.1	Test Schedule . . . . .	49
7.2	Testing Objectives . . . . .	50
7.3	System Testing . . . . .	51
7.4	Flight Test Schedule and Plan . . . . .	54
7.5	Flight Checklist . . . . .	54
<b>8</b>	<b>Performance Results</b>	<b>55</b>
8.1	Demonstrated System Performance . . . . .	55
8.2	Demonstrated Aerodynamic Prototype Flight Performance . . . . .	59
<b>9</b>	<b>References</b>	<b>60</b>

## Abbreviations, Acronyms, and Symbols

- ABS: Acrylonitrile butadiene styrene
- ac: Aerodynamic Center
- APC: APC Propeller Company
- AVL: Athena Vortex Lattice
- $b$ : Wing Span
- BB: Ball Bearing
- BEC: Battery Elimination Circuit
- BWB: Blended Wing Body
- $c$ : Chord Length
- CAD: Computer Aided Design
- $C_i$ : Coefficient of Generic Quantity
- CFD: Computational Fluid Dynamics
- CG: Center of Gravity
- CNC: Computer Numerical Control
- $D$ : Drag Force
- $e$ : Oswald's Efficiency
- ESC: Electronic Speed Controller
- FEA: Finite Element Analysis
- $F_P$ : Propeller Normal Force
- $g$ : Gravitational Acceleration
- GA: Genetic Algorithm
- GM: Ground Mission
- $i$ : Angle of incidence
- $I$ : Current
- $l$ : Longitudinal Length
- $\bar{l}$ : Generic Quantity  $l$  Normalized to MAC
- $L$ : Lift Force
- LED: Light Emitting Diode
- LiPo: Lithium-Polymer (often refers to batteries)
- $M$ : Moment
- $m$ : Mass
- $m_{fuse}$ : Slope of Fuselage Moment Coefficient Curve.
- np: Neutral Point
- PDB: Power Distribution Board
- PLA: Polylactic Acid
- PU: Power Unit—a Combined Unit of 1 Motor, 1 Prop, and 1 ESC
- PVC: Polyvinyl Chloride (Foam)
- PWM: Pulse Width Modulation
- $RPM$ : Revolutions per Minute
- Rx: Receiver
- SOP: Standard Operating Procedure  $S_{ref}$ : Planform Area
- $T$ : Thrust Force
- TO: Topology Optimization
- TOFL: Takeoff Field Length
- UW: University of Washington
- $v$ : Velocity
- $W$ : Weight
- XPS: Extruded polystyrene
- $z$ : Vertical Distance
- $\alpha$ : Angle of Attack (AOA)
- $\delta$ : Control Surface
- $\epsilon_d$ : Downwash
- $\epsilon_u$ : Upwash
- $\zeta$ : Dynamic Mode Damping Ratio
- $\eta$ : Lifting Surface to Freestream Dynamic Pressure Ratio
- $\tau$ : Dynamic Mode Period
- $\omega$ : Dynamic Mode Angular Frequency

# 1 Executive Summary

The objective for the 2020-2021 American Institute of Aeronautics and Astronautics (AIAA) Design Build Fly (DBF) competition is to design, build, and test an unmanned aerial vehicle (UAV) and associated deployable, towed sensor. Missions will include a proof of flight demonstration, a high-capacity transport mission, and an operational mission where the aircraft must deploy (from internal storage), operate (LED lights in a predetermined sequence), and retrieve (by retracting) a towed sensor. The primary requirements of the aircraft are that it adheres to the codes specified in the Federal Aviation Administration (FAA) Part 107 standards, carries less than 200 Watt-hours of energy, and is not of vertical-takeoff or lighter-than-air configuration. Furthermore, as imposed by the AIAA, the wingspan is limited to five feet and the sensor must have a minimum aspect ratio of 4:1.

This year, the Huskyworks DBF team focused on optimizing the design of the aircraft in three main areas. The Aerodynamics team determined that the optimal configuration for both a high-capacity and high-endurance aircraft would be a tandem wing. Despite the divergence from traditional design methodologies, this was chosen to maximize the lift and endurance of the aircraft while staying within the five feet wingspan limit. This allowed for the accommodation of a larger, high-capacity fuselage. In order to maximize the internal storage capacity of this fuselage, the Materials team designed a monocoque composite sandwich structure frame. A carbon-Kevlar, 0/90 degree twill-woven sheet was chosen for the matrix element while a 0.125 inch thick closed-cell PVC scored foam sheet was chosen for the sandwich core. This eliminated the need for internal ribs and maximized the payload capacity of the aircraft while maintaining a high strength-to-weight ratio. In order to provide the required thrust for the aircraft and ensure high performance mission flights, the Propulsion team sourced high-efficiency components from the FPV industry. By bringing these components into the fixed-wing scene, the team saw a vast increase in propulsion efficiency and performance over the fixed-wing standards. A tri-motor design was chosen to maximize endurance for Mission 3 while providing a competitive top speed for Mission 2.

The Huskyworks aircraft, *Dragonfly* shown in Figure 1 is designed to operate as either a high-endurance or high-capacity and high-speed aircraft depending on the mission requirements. *Dragonfly* will takeoff with an empty weight of 23 pounds (Mission 1) and with a fully-loaded weight of 44 pounds (Mission 2). For Mission 2, the aircraft is designed to fly with a payload of 18 sensor boxes with a top speed of 78 mph (35 m/s) and will complete three laps in 96 seconds. For Mission 3, in order to fly for the full time, the aircraft will cruise at 58 mph (26 m/s) and will tow, operate, and retrieve an 18 inch long, one pound sensor. Large loading doors and a removable empennage ensure that *Dragonfly* can complete the ground mission in less than 120 seconds.

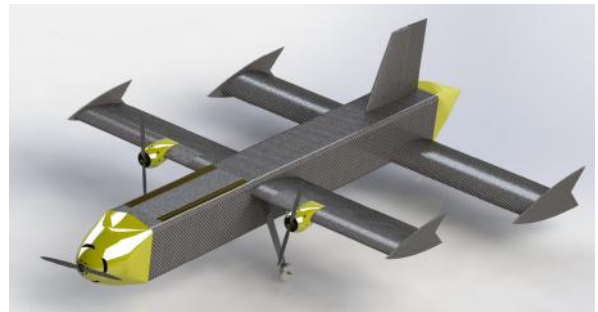


Figure 1: The Dragonfly

## 2 Management Summary

The 2020-2021 team consists of 50 students who participate in an extracurricular manner. The team is made up of seven seniors, five juniors, and thirty-eight underclassmen. During the autumn quarter, in addition to these members, six seniors in the aeronautics and astronautics program aided in the conceptual design of the aircraft. The team is led by a leadership team consisting of eleven returning members that were selected via a team-wide election. Operations, design, and testing efforts conducted by the team are planned and carried out by its leadership team and members, with limited support from the faculty advisors.

### 2.1 Team Organization

The Huskyworks team is organized with a leadership structure similar to most aerospace companies. Four senior (in experience not class standing) leads are responsible for establishing the vision and direction of the club, while the other seven leads are each responsible for a mission-critical subsystem team.

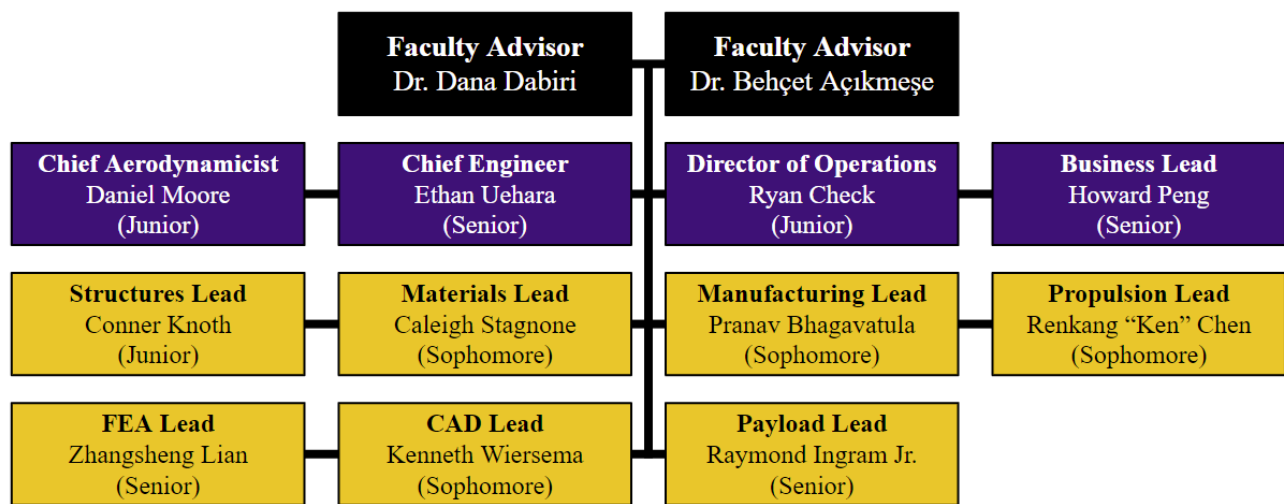


Figure 2: Huskyworks Team Management Chart

The Chief Engineer is tasked with organizing the general design process, interfacing between the team and the department, and establishing the overall vision of the club. While the Chief Engineer leads the overall design phase, the Chief Aerodynamicist is specifically responsible for leading the aerodynamic configuration analysis. The Director of Operations organizes the day-to-day activities by setting up meetings and coordinating documentation and logistics. The Business Lead is responsible for sourcing industry sponsorships, organizing the team fundraiser, and submitting purchase requests. The other subsystem leads are each responsible for a specific facet of design and a cohort of members, serving as an intermediary between the team members and the senior leadership.

## 2.2 Milestone Chart

The milestone chart is used to plan tasks, allocate members to high-priority areas, and track project progress. The chart is broken up into three main phases with the design phase in the fall, the manufacturing phase in the winter, and the flight-testing phase mainly in the spring. Progress is tracked and the chart is continually updated in order to maintain an accurate representation of progress. Additionally, there are five major milestones that are the primary indicators of success (marked as stars in the milestone chart in Figure 3).

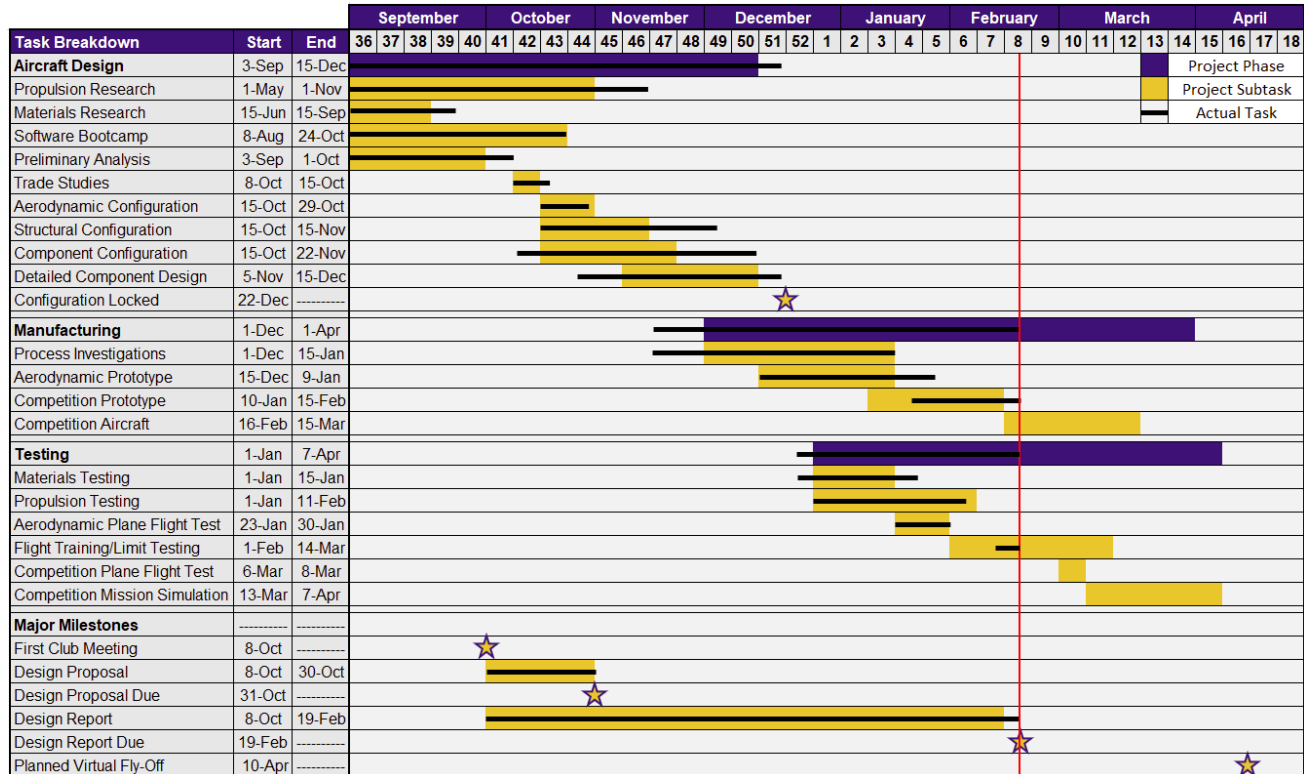


Figure 3: Huskyworks Team Milestone Chart

## 3 Conceptual Design

During the conceptual design phase, the team analyzed the requirements for each mission and developed a scoring optimization algorithm to guide the design. This information was used to enable exploration of design options and determine design requirements and key performance indicators for each of the aircraft subsystems,

### 3.1 Mission Requirements and Constraints

The goal of the 2020-2021 competition is to develop, manufacture, and fly a UAV capable of both deploying and operating a sensor mid-flight, as well as carrying a payload of sensors. The aircraft, of a wingspan less than five feet, must operate with a commercial propulsion system under a 200 Watt-hour energy limit. Additionally,

the aircraft cannot use a rotary or lighter-than-air configuration and cannot have external takeoff assistance or components that fall from the aircraft during flight. The sensor must remain aerodynamically stable through the duration of its deployment, operation, and recovery. The sensor must also have a minimum diameter of one inch and a minimum length-to-diameter ratio of 4:1.

For each flight mission, the aircraft will fly in a clockwise racetrack pattern. After its first 180° turn during each lap, the aircraft must also complete a 360° turn before continuing on its flight path. A schematic of this flight path is shown in Figure 4.

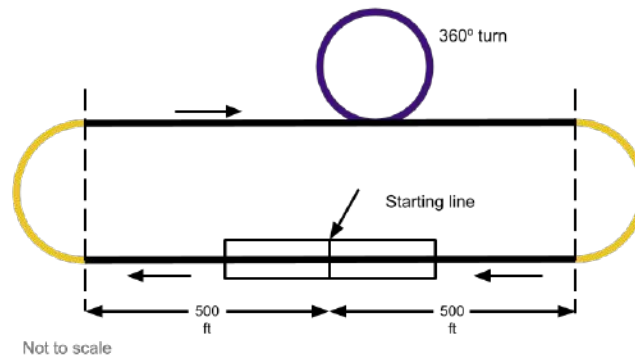


Figure 4: AIAA DBF Lap Layout

All flight missions are given a take-off field length of 100 feet. Additionally, the aircraft must complete a successful landing to receive a score.

### 3.1.1 Competition Scoring Summary

The score will be computed from the Written Report Score and Total Mission Score as given by Equation 1.

$$SCORE = \text{Written Report Score} \cdot \text{Total Mission Score} \quad (1)$$

The Written Report Score is calculated on a 100-point scale and is based on the quality of the design report. The Total Mission Score is the sum of the scores for Mission 1 ( $M_1$ ), Mission 2 ( $M_2$ ), Mission 3 ( $M_3$ ), and the Ground Mission ( $GM$ ). The Total Mission Score is given by Equation 2.

$$\text{Total Mission Score} = M_1 + M_2 + M_3 + GM \quad (2)$$

### 3.1.2 Mission Scoring Breakdown

#### Mission 1: Staging Flight

Teams must complete 3 laps within a 5-minute flight window without any payload. Time starts when the throttle is advanced for the first takeoff or attempted takeoff. Teams will receive a score of 1.0 ( $M_1 = 1.0$ ) for a successful attempt and a score of 0.0 ( $M_1 = 0.0$ ) for an unsuccessful attempt.

### Mission 2: Delivery Flight

Teams must complete three laps as quickly as possible while carrying a payload of the sensor in the shipping container, simulated shipping containers, and sensor deployment and recovery mechanism. The score for Mission 2 is a function of shipping containers / flight time. Time begins when the throttle is advanced for takeoff or first attempted takeoff. The Mission 2 score is given by Equation 3.

$$M_2 = \frac{\left(\frac{N_{containers}}{T_{M_2}}\right)_{UW}}{\left(\frac{N_{containers}}{T_{M_2}}\right)_{max}} \quad (3)$$

$\left(\frac{N_{containers}}{T_{M_2}}\right)_{UW}$  is the University of Washington's ratio of number of containers to Mission 2 time and  $\left(\frac{N_{containers}}{T_{M_2}}\right)_{max}$  is the maximum ratio of the number of containers to Mission 2 time for the highest-scoring team in that category.

### Mission 3: Sensor Flight

Teams must complete as many laps as possible within a 10-minute window while deploying, towing, and recovering the sensor. Time begins when the throttle is advanced for takeoff or first attempted takeoff. The sensor must be fully deployed before the first 360° turn. After the final 360° turn, the sensor must be recovered. The sensor does not need to be fully recovered prior to crossing the finish line, but it must be fully recovered inside the aircraft before landing. The score for Mission 3 is given by Equation 4.

$$M_3 = \frac{(N_{laps} \cdot l_{sensor} \cdot w_{sensor})_{UW}}{(N_{laps} \cdot l_{sensor} \cdot w_{sensor})_{max}} \quad (4)$$

$(N_{laps} \cdot l_{sensor} \cdot w_{sensor})_{UW}$  is the University of Washington's product of laps flown, sensor length, and sensor weight.  $(N_{laps} \cdot l_{sensor} \cdot w_{sensor})_{max}$  is the max product of those of the highest scoring team.

### Ground Mission: Operational Demonstration

Teams must demonstrate the performance of the shipping container, the loading and unloading of Mission 2 payload, and deployment and recovery of the sensor. The sensor shipping container will be dropped on all sides from a height of 10 inches. The sensor will be removed from the shipping container and the assembly crew member will demonstrate that the sensor has not been physically damaged. For the timed mission, the assembly crew member will load and unload the Mission 2 payload and load the Mission 3 payload. The scoring for the Ground Mission is given by Equation 5.

$$GM = \frac{t_{min}}{t_{UW}} \quad (5)$$

$t_{min}$  is the fastest Ground Mission time for all teams and  $t_{UW}$  is the University of Washington's fastest Ground Mission time. After the timed mission, the deployment and recovery of the sensor will be demonstrated by the pilot and assembly crew member.

### 3.2 Design Parameters and Constraints

The aircraft must meet the following requirements.

Configuration:

- Maximum allowable wingspan is 5 feet.
- The aircraft may not be of rotary or lighter-than-air configuration.
- No structure/components may be dropped from the aircraft during flight.
- Must be propeller driven and powered by off-the-shelf electric motor(s). Motors may be any commercial brushed or brushless electric motor.
- The aircraft must use commercially produced propellers. Teams may modify the diameter of the propeller or paint the propeller. No other propeller modifications are allowed.
- The aircraft must have an externally accessible switch to turn on the radio control system.
- No externally assisted takeoff is allowed (takeoff must happen in less than 100 feet).

Batteries:

- Batteries must be Nickel-Cadmium (NiCd), Nickel-metal hydride (NiMH), or Lithium-polymer (LiPo).
- Teams must choose only one battery type for propulsion.
- Teams may use any battery type to power the receiver, transmitter, and servos.
- The propulsion package may not exceed 200 Watt-hours of stored energy.
- LiPo battery requirements:
  - LiPo Battery packs must be commercially procured and unmodified.
  - If more than one battery pack is used for a single purpose, all battery packs must be identical and connected in parallel.

Payload:

- The sensor must have a diameter of at least 1 inch and a length-to-diameter ratio of at least 4:1.
- The sensor must be aerodynamically stable during deployment, operation, and recovery.
- The sensor and sensor deployment/recovery mechanism must be carried internally to the airplane.
- The sensor must fully fit inside the sensor shipping container.
- The sensor shipping container must protect the sensor from drop shock events.
- The sensor shipping container simulators must be the same size and at least the same weight as the sensor shipping container with sensor.
- The sensor must have three external lights that can be viewed while in the deployed position during flight.
  - The lights must be turned on and off via the flight or payload transmitter.
  - The lights must be controlled by a physical connection to the airplane through the tow cable.
  - The sensor must contain its own power supply.

### 3.2.1 Score Analysis

By examining the 2020-2021 mission requirements and scoring equations, design objectives were developed that would maximize the total score. These design objectives led the creation of the scoring model which directed the optimization of the conceptual design, and ultimately determined the aircraft's configuration.

The scoring analysis was approached from a statistical perspective, distinguished from the traditional deterministic point of view, such as solely relying on equation derivations. Specifically, the team developed a mathematical flight model and used a Genetic Algorithm (GA) to optimize it to determine the best configurations. To conclude the analysis, all parameters of each configuration were altered to test their sensitivity to the overall score.

The mathematical flight model was the baseline of the numerical analysis. The team started with force and power balance equations, then combined them with empirical formulae from previous years, for example, the thrust produced from motor candidates. This basic model was then outfitted with equations identified in the mission scoring breakdown (Equations 2 to 5) to create the performance evaluation score as a real number. The Ground Mission and Mission 1 parameters were omitted in this analysis because they contributed little to the synoptic-scale evaluations. The following are some representative equations that relate the mathematical model to the competition.

$$N_{sensor} = \left\lfloor \frac{c_L \cdot S_{wing} \cdot \rho_0 \cdot v_{m2} - w_{aircraft}}{w_{sensor}} \right\rfloor \quad (6)$$

$$M_2 = \begin{cases} \frac{N_{sensor} \cdot v_{M2}}{3L_{course}}, & t_{m2} = \frac{3L_{course}}{v_{M2}} \leq 300 \text{ s} \\ 0, & otherwise \end{cases} \quad (7)$$

$$M_3 = \left\lfloor \frac{(600 \text{ s}) \cdot v_{m3} \cdot L_{sensor} \cdot w_{sensor}}{L_{course}} \right\rfloor \quad (8)$$

After building the mathematical model, the team fed it into the GA to seek out the optimal configurations. GA is a search process inspired by Charles Darwin's theory of natural selection, in which the fittest individual is selected to reproduce the next generation. During the reproduction, a Gaussian noise was added to each parameter to mimic the genetic mutation. Next, the mathematical model calculated the entire generation's evaluation score to select the best, and the process was repeated until convergence. However, GA is also an iterative process in which the team has to change the hyperparameters and constraints to compare different outputs. Since the mathematical model's convexity is not guaranteed, i.e., multiple local minima existed in the domain, the team started with overestimated constraints, where no individual survived. Then, the harsh restrictions were gradually relaxed until there were acceptable configurations. The team executed each iteration several times to reduce the algorithm's randomness. In conclusion, the team chose the hyperparameters of simulating 50 generations with a size of 10,000 in which only 200 individuals survived.

Testing the sensitivity of the parameters was also a statistical process. The team introduced a multiplier to all parameters and recorded the score changes for every 200 survived individuals. Then, the average score changes

were plotted in order to serve as general guidance in the latter configuration selection. As a result, the testing algorithm produced various plots and two of the many representative samples are listed below. For example, Figure 5 shows the sensitivity of the wing chord length. An important takeaway is that a longer chord had more drag which reduced velocity, and lowered the overall score. However, decreasing the chord length reduced the lift, which caused more sample configurations to break the constraints, i.e. lowering the validness ratio. In addition, the staircase-like Mission 3 score was likely produced by Equation 8.

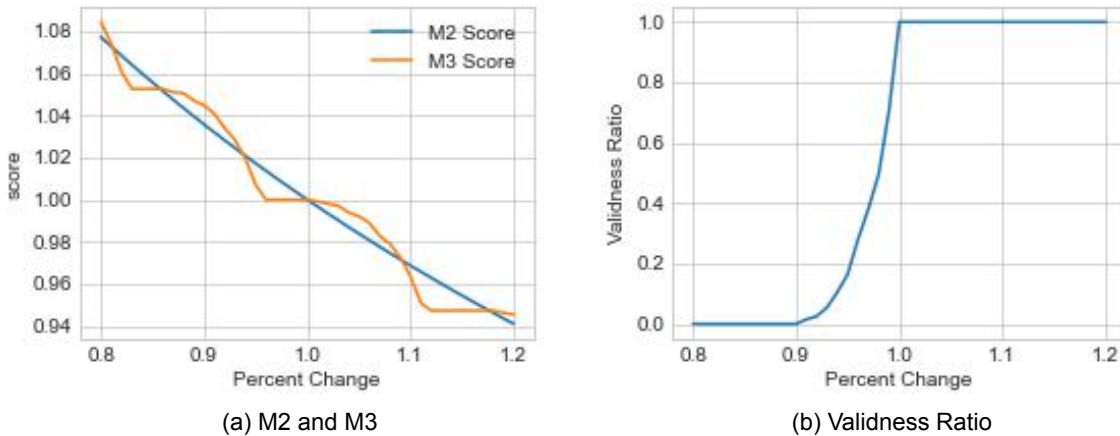


Figure 5: Impact from Parameter: Wing Chord Length

In Figure 6, the coefficient of lift ( $C_L$ ) did not affect the score within the 20% window, but altering it significantly lowered the validness ratio because a reduced  $C_L$  means less lift generated, thus fewer sensors can be carried in Mission 2; and an increased  $C_L$  means too much lift is generated, thus velocity is decreased. It is important to note that the model did not account for the potential variance of angle of attack due to the need to streamline the analysis.

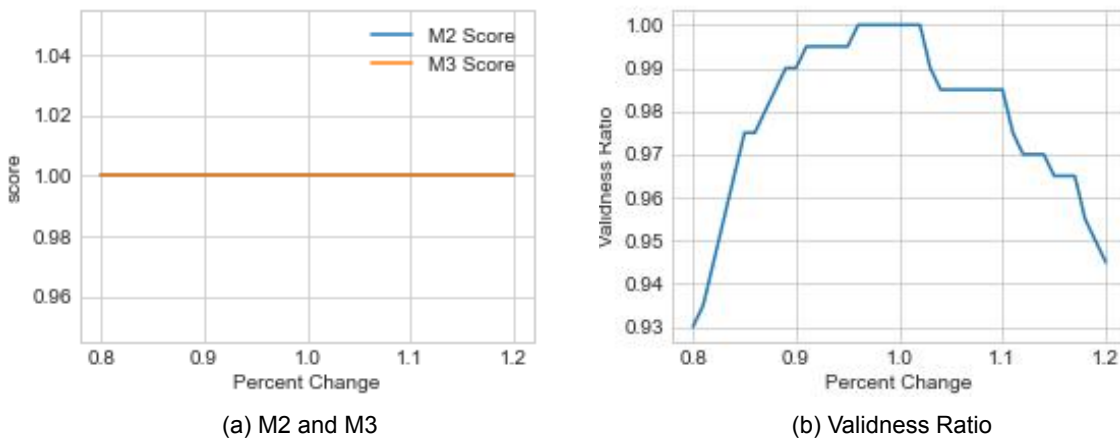


Figure 6: Impact from Parameter: Coefficient of Lift

### 3.2.2 Performance Analysis

The survival configurations from the GA Scoring Analysis Section provided the foundation of the Performance Analysis. However, due to the randomness of the algorithm, an individual configuration did not offer statistical significance. Therefore, post-processing of the data required averaging multiple individuals to yield a more dependable result. K-mean Clustering (one form of an unsupervised machine learning algorithm) was selected in response to the specifications above. It separates data into  $k$  clusters (groups) according to their likeliness, with the centroid of each cluster being their average.

After normalizing all parameters by reducing to Z-score ( $\mu = 0, \sigma = 1$ ), the team executed the algorithm with hyperparameter  $k$  from 1 to 19. The marginal return of percent variance reduced significantly after  $k = 4$ , i.e., separating data into more clusters did not reduce the data scattering. Therefore, the data naturally divided into four groups. Table 1 is the result of four different centroids, which were the configurations selected by the GA.

Table 1: GA Optimized Parameters by Centroid Number

No. of Centroids	Plane Weight (lb)	Velocity M2 (ft/s)	Velocity M3 (ft/s)	C.L Cruise	Prop Diameter (in)	Power (W)	Chord (in)	Sensor Weight (lb)	Number of Sensors	M2 Predicted Score	M3 Predicted Score	Total Score
0	15.5	96	98	0.80	15.3	229	22	2.14	18.9	1.61	2.16	4.77
1	15.3	95	96	0.97	13.4	418	23	2.13	19.3	1.61	2.14	4.75
2	15.5	96	97	1.05	13.8	298	21	2.14	19	1.60	2.15	4.75
3	15.6	97	98	1.06	13.1	416	22	2.10	19.2	1.62	2.14	4.76

The GA outputted a set of suggested performance values for the aircraft. Since the GA approach was done in an ideal and optimized case, the weight of the aircraft and fully loaded Mission 2 payload summed to 55 pounds. In reality, this was determined to be outside of the ability of the team and modifications had to be made to what was generated by the GA and what was selected for the final parameters for the *Dragonfly*.

The GA also predicted a very low airframe weight of about 15.5 pounds. Upon analysis of the base components and necessary structural materials needed to support such a heavy aircraft, the team determined that the estimated structural weight was too low and 20 pounds was a more accurate estimate. Furthermore, the results of the configuration analysis led the team to look at a tandem configuration which was something that the GA did not account for when determining the size of the chord. After a brief look at the trade study for the propulsion selection, the team decided to keep the number of carried sensors for Mission 2 the same while reducing the weight of each individual sensor to approach a more reasonable Mission 2 aircraft weight.

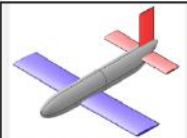
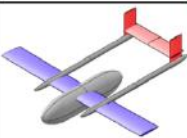
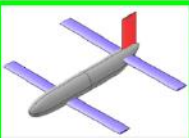
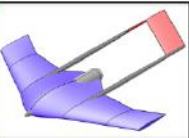
After accounting for the needed modifications to the GA, the team took the remaining parameters and set those as target values during the preliminary design of the aircraft. Those parameters ultimately drove many of the decisions during the configuration selection phase and guided the design methodology approach.

### 3.3 Configuration Selection

#### 3.3.1 Aerodynamic Configuration Selection

Configuration analysis of the three proposed designs consisted of obtaining qualitative estimates on performance parameters, and of qualitative comparison between the design configurations. These geometric configurations had comparable total lengths, identical wingspans and wing-areas, and identical tail areas. The scoring for each of the Figures of Merit was based upon data generated from VSPAero and formulas found in (1), (2), (3).

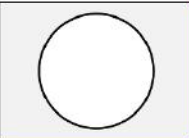
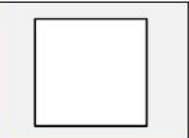
Table 2: Aerodynamic Configuration Selection

					
Figures of Merit	Factor	Low-Wing Conventional	High-Wing Twin-Boom	Tandem	BWB
Endurance	0.25	7	8	10	6
Complexity	0.25	10	7	7	4
Wing Loading	0.20	8	8	8	8
Max L/D	0.15	7	8	10	7
Sref Flexibility	0.15	5	5	9	7
	<b>Total</b>	<b>7.7</b>	<b>7.3</b>	<b>8.7</b>	<b>6.2</b>

Since the competition rules limited the span to 5 feet, the ability to preserve aspect ratio while simultaneously increasing the wing area ( $S_{ref}$ ) lead to a high score for the tandem wing overall. Although the payload capacity is comparable, the tandem wing would likely provide a higher Mission 2 score than a mono-wing. Wing area could be increased for the mono-wing configurations, but with the span constraint, the chord would have to increase. This would increase the risk of flow-separation and aerodynamic performance degradation. In contrast, the thinner chords of a tandem wing with the same  $S_{ref}$  may be increased while retaining superior performance.

#### 3.3.2 Fuselage Geometry

Table 3: Fuselage Cross-Section Selection

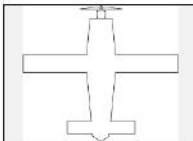
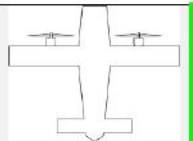
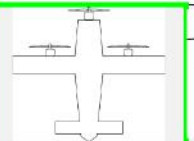
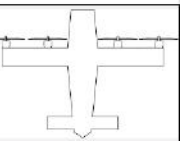
				
Figures of Merit	Factor	Circular	Filletted Square	Square
Low Drag	0.1	10	7	5
Interface	0.2	4	9	9
Ease of Mfg.	0.3	7	8	7
Strength	0.2	9	8	7
Capacity	0.2	7	8	9
	<b>Total</b>	<b>7.1</b>	<b>8.1</b>	<b>7.6</b>

As shown in Table 3, three shapes were considered for the cross section of the fuselage: a circle, square, and filleted square. The circular shape provided the best aerodynamic performance, but it was more difficult to manufacture and had less internal storage space compared to the others. The square shape had a large internal capacity, but it caused a more significant increase in drag. The rounded square was optimal because although it has a roughly 200% increase in drag in comparison to the circular, the actual magnitude of the drag was small versus the increase in capacity and manufacturability (4).

### 3.3.3 Propulsion System Selection

The number of motors has the greatest influence on the design of the aircraft since the aircraft must accommodate the propulsion system and utilize it without exceeding the limits. Therefore, this is one of the first factors to be confirmed regarding the aircraft. To confirm the exact number of motors for the system, the following table was made with the scores factored in from performance data provided by manufacturers and weighted by their importance as voted by the team. In addition, note that the components in each configuration have been optimized for the best overall score, therefore, the size or model of the motors for each configuration may be different. As shown in Table 4, the Tri-Motor configuration won primarily due to the Mission 2 thrust requirements.

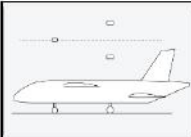
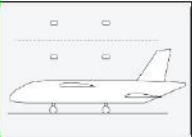
Table 4: Propulsion System Configuration Selection

					
Figures of Merit	Factor	1 Motor	2 Motor	3 Motor	4 Motor
Thrust M2	0.4	5	8	10	7
Thrust M3	0.3	6	10	9	8
Weight	0.1	10	7	8	6
Complexity	0.1	10	9	8	7
Cost	0.1	10	7	8	7
	<b>Total</b>	<b>6.8</b>	<b>8.5</b>	<b>9.1</b>	<b>7.2</b>

### 3.3.4 Landing Gear Selection

After trade study and further research, there were three main types of landing gear configurations taken into account: tricycle, taildragger and quadricycle. With regards to the taildragger gear, one important distinction was the location of the gear mount - be that on the underside of the wing or underside of the fuselage. This was important to consider since the angle of attack upon takeoff would be vastly different depending on the mount location (when using pre-made, purchased gear). Due to past competition experience, a heavy weight factor was placed on the ability to steer the aircraft while on the ground. This coupled with the weight factor caused the quadricycle gear to score poorly in Table 5. Ultimately, the combination of pitch angle factor and maneuverability led the team to choose the wing-mounted taildragger gear.

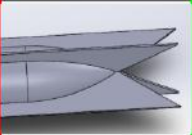
Table 5: Landing Gear Configuration Selection

					
Figures of Merit	Factor	Tricycle	TD Low Mount	TD Wing Mount	Quadricycle
Weight	0.2	8	9	9	4
Maneuverability	0.3	6	8	8	4
Strength	0.1	6	7	8	10
Pitch Angle	0.2	7	5	9	7
Drag	0.2	7	8	8	4
	<b>Total</b>	<b>6.8</b>	<b>7.5</b>	<b>8.4</b>	<b>5.2</b>

### 3.3.5 Sensor Design

With regards to the sensor design, it was determined that the stability fins would have the largest impact on the configuration of both the sensor and the sensor storage box. The two primary factors were stability and packability (referring to the ease of storage within the sensor box). Due to the ability to collapse a large surface area fin into a small cross-section, the Retractable fin design was the clear winner. To preface Table 6, it is important to note that the configuration discussion happened before the rule clarification was released. Therefore, the legality row was added as a go/no-go element in January after the bulk of the testing had already been done with the Retractable fins. Therefore, even though the Retractable design won initially, the team ultimately went with the Conventional style in order to remain within competition guidelines.

Table 6: Sensor Fin Configuration Selection

					
Figures of Merit	Factor	RPG	Retractable	Full-Body	Conventional
Stability	0.4	5	10	3	7
Packability	0.2	10	10	10	7
Complexity	0.2	7	5	10	10
Space	0.1	7	5	10	10
Drag	0.1	5	8	2	5
Legality	Yes/No	No	No	Yes	Yes
	<b>Total</b>	<b>6.6</b>	<b>8.3</b>	<b>6.4</b>	<b>7.7</b>

### 3.3.6 Sensor Storage Box Design

XPS, PVC, and Polyurethane foam were investigated for impact resistance within the sensor storage container. As PVC foam is primarily used to increase stiffness, it did not provide enough impact resistance. Polyurethane was chosen over XPS because it would yield not puncture due to the sensor fins when dropped.

Table 7: Sensor Storage Box Material Selection



Figures of Merit	Factor	XPS Foam	Polyurethane	PVC Foam
Shock Damping	0.4	7	10	5
Ease of Mfg.	0.4	7	8	7
Cost	0.2	8	7	8
	<b>Total</b>	<b>7.2</b>	<b>8.6</b>	<b>6.4</b>

### 3.4 Final Conceptual Design Configuration

The final configuration for the *Dragonfly* is a tri-motor, tandem wing aircraft that is designed to carry a total of 18, 1.4 pounds sensor boxes on Mission 2 and fly 17 laps (35 seconds per lap) for Mission 3. The *Dragonfly* will tow a 18 inch, one pound sensor for Mission 3 that will self-stabilize using Conventional fins. The *Dragonfly* will use a taildragger-style landing gear in order to maneuver during ground roll while also preserving an optimal angle of attack upon takeoff.

## 4 Preliminary Design

### 4.1 Design Methodology

The Huskyworks team designed the *Dragonfly* aircraft with input from team members across the aerodynamic, structures, and propulsion teams. The team designed an aircraft that maximized the sensor storage capacity for Mission 2 and the number of laps completed for Mission 3, as well as minimized the loading time during the Ground Mission. The desired capabilities of the *Dragonfly* were determined by the GA optimization studies and performance analysis.

The aerodynamics team analyzed several airfoils based on several factors, including stability, stall angle, lift, and drag that would produce the required lift for Mission 2. As a tandem wing configuration is uncommon, a large emphasis was placed on analyzing the stability of the aircraft; the team built an aerodynamic prototype to prove that the configuration was stable. Additionally, the aerodynamics team investigated sensor stability and configuration. The structures team compared a monocoque and semi-monocoque structure, as well as various carbon-fiber, Kevlar, and fiberglass fabrics for structural strength. To maximize the Mission 2 score through increasing internal storage capacity, the team selected a monocoque fuselage structure fabricated using a composite sandwich structure of carbon-Kevlar fabric and PVC foam. The propulsion and avionics team configured a 200 Watt-hour compliant propulsion system that met the performance goals of Mission 2 and 3. They also designed the operational features of the sensor and a light-weight electronics system for the aircraft.

## 4.2 Design Trade Studies

### 4.2.1 Wing Planform and Aircraft Sizing

The wing planform was designed to provide sufficient lift to allow takeoff in under 100 feet while still offering manufacturing simplicity. Due to a lack of compressibility effects, each wing was made rectangular and of equal area. With the span of the wings rule-constrained to 5 feet, wing area variation was controlled by the chord. In order to maintain a theoretical Oswald's efficiency of 0.9 (90% efficiency relative to an elliptical wing lift distribution), the chord was sized to 12 inches, for an Aspect Ratio of 5 (1).

Aircraft sizing was based upon the design region of Figure 7. Constraints on this design space included a conservative 90-foot Mission 2 TOFL, a  $C_{L,max} = 1.5$ , a maximum 3g loading,  $C_{D0} \approx 0.0238$ , and  $V_{stall} \leq 50$  ft/s for pilot comfort (1). With Mission 2 score proportional to the number of sensors and thus payload weight, and the Mission 3 score proportional to the sensor weight, the optimal design occurred at the highest wing-load ( $W/S$ ) allowed by the available thrust. With an initial predicted minimum available thrust of 18 pounds, the preliminary aircraft weight was determined to be 37.3 pounds. Later increases in weight due to manufacturing tolerances and desired payload accommodation were accounted for with iterative sizing of the PU, per Section 4.2.3.

### 4.2.2 Vertical Stabilizer

The vertical stabilizer was designed to provide yaw stability during flight. The initial sizing process followed the stabilizing surface coefficient method (5). This value takes into account the fuselage length, location from the center of gravity, and surface area of the fuselage side to determine the sizing needed to properly stabilize the aircraft in the yaw axis. However, after the first Aerodynamic Prototype flight test, it was apparent that the stabilizer needed to be resized and that Equation 9 was insufficient.

$$S_{vt} = \frac{K_v S_B L}{\eta_F \rho \frac{dC_{L,F}}{d\psi}} \quad (9)$$

The design was then changed to follow the more standard volume coefficient model used in Raymer as opposed to the stabilizing surface coefficient method in the Diehl text, where the information about the sizing was found empirically, since the empirical data was taken from more "conventional" configurations that did not appropriately describe the performance of the non-conventional tandem wing aircraft.

The suspected differences between the data provided in Diehl were primarily in the effects of the rounded rectangular fuselage and the vastly different aerodynamic behaviour over the trailing wing. With these effects not

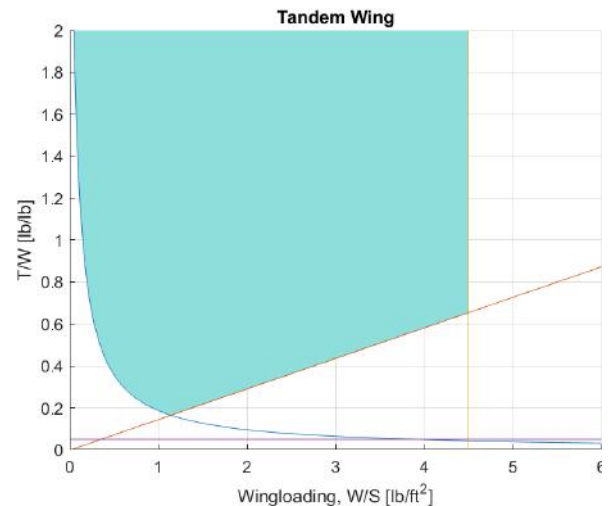


Figure 7:  $W/S - T/W$  Aircraft Sizing Diagram

accounted for in Diehl, it's suspected that the values provided in the text were not sufficient to appropriately describe the sizing. The updated method for the vertical tail sizing followed the more traditional design method of volume coefficients found in Equation 10 (1).

$$C_{VT} = \frac{L_{VT}S_{VT}}{b_W S_W} \tag{10}$$

Due to the fuselage design being effectively finalized, it was best to use the information generated in the CAD file to account for the lengths required for the volume coefficient. A value of  $C_{VT} = 0.08$  was used to describe the vertical tail size. This value is similar to a twin turboprop aircraft, which was the most appropriate due to the propulsion system that was designed. The previous design used a volume coefficient of  $C_{VT,old} = 0.03$ , which provided a much smaller area.

With the new equation in place, and a volume coefficient clarified, a new design that accounted for existing structural support and available material had to be designed. The control surface sizing was still sufficient from Diehl and was kept from the previous iteration and effectively scaled to the new design. The area used in the second prototype was still slightly less area than recommended by the equation to ensure that the vertical stabilizer did not have any significant impact on the CG, and still adhered to the existing support structure provided in the earlier iteration of the vertical stabilizer.

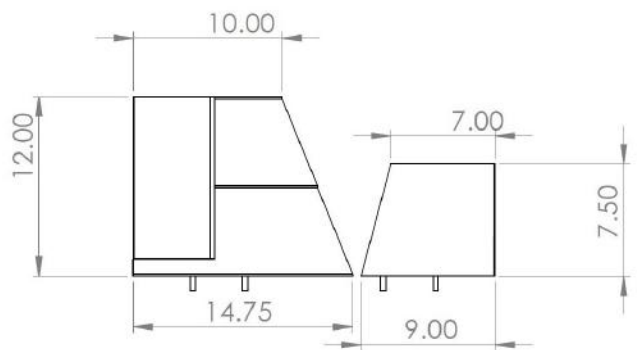


Figure 8: Vertical Stabilizer Resized Dimensions

### 4.2.3 Propulsion Sizing

The governing principle of the propulsion system was high efficiency. 200 Watt-hours of energy must be converted into as much thrust, speed, and flight time as possible. Therefore, the design choices were based on the maximum allowable energy consumption and followed the flowchart (Figure 9).

In the first step, both the quality (discharge rate, voltage, etc.) and quantity of available energy were determined, where quality was a property of battery formula and cell arrangement (in parallel or in series) and quantity was a property of cell size. After investigation, LiPo batteries were chosen for their vastly superior energy density and discharge rate to other options listed by the regulations.

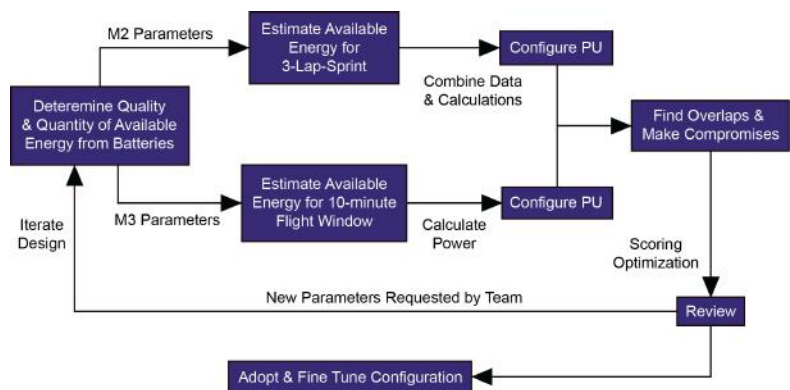


Figure 9: Propulsion Optimization Process

After LiPo batteries were selected, the overall propulsion system was investigated separately for capabilities in Mission 2 and Mission 3. For Mission 2, it was estimated that 44 Watt-hours of energy needed to be reserved for takeoff, landing, and a potential go-around, while the system would use all 156 Watt-hours of available energy for the 3-lap sprint, or 52 Watt-hours per lap. Meanwhile, for Mission 3, after combining both the effects of a significantly reduced load and additional energy consumed for sensor deployment and retraction, it was estimated that again 44 Watt-hours of energy needed to be reserved, leaving 156 Watt-hours for the 10-minute cruise. Since Mission 3 was time-limited, staying airborne for as much of the 10-minute window as possible would result in a higher lap count and thus a higher score. By the calculation, it was determined that power drawn by the system during flight must not exceed 936 Watts. Note that due to the lack of dynamic thrust and velocity data, it was decided that static data would be used, and the result multiplied by a factor of safety to account for reality.

For the propulsion calculations the following definitions were outlined:

- $P$  is the average electrical power draw by the system.
- $E$  is energy limit per lap, or 53 Watt-hours.
- $d_S$  is the total distance of the straights in a lap, or 2000 feet.
- $\omega$  is rotational velocity of the motor, found in the manufacturer's data.
- $k$  is the pitch of the prop used by the motor.
- $F$  is the factor of safety to account for non-ideal conditions (reality).
- $a$  is the centripetal acceleration possible by the airframe.

$$P = \frac{E}{\frac{d_S}{(\omega \cdot k \cdot F)} + \frac{4\pi(\omega \cdot k \cdot F)}{a}} \quad (11)$$

Afterwards, extensive research was conducted to configured components according to the derived Equation 11 using  $P$  as the independent variable and matching data provided by manufacturers (6) (7) (8). The top 5 thrust-producing systems were chosen as a set of candidates for both missions.

Table 8: Top Three Candidate Motors

	Motor	M2 Propeller	M3 Propeller	Battery
Option 1	T-Motor AT3530 580KV	APC 13x11	APC 14X10	SMC 6S 4500mAh
Option 2	iFlight X4214 660KV	APC 12X12	APC 13X10	
Option 3	Scorpion 4020 540KV	APC 13X11	APC 14X10	

Eventually, the two sets of candidate systems identified for Mission 2 and Mission 3 were combined and scored, and the three highest scoring options were sent to the general team for evaluation of impact on structures, flight envelope, and manufacturing. Three options of different motors were chosen to be further investigated and bench tested to confirm performance predictions, establish load correlations, and simulate mission runs. Table 8 summarizes the options presented to the team after the propulsion sizing trades.

### 4.2.4 Fuselage Structure

Typical airliners have a semi-monocoque fuselage structure. This is largely due to the need for high stiffness with a minimal increase in weight. However, the ability to manufacture a composite sandwich structure fuselage allowed the Huskyworks team to consider a monocoque fuselage structure. A trade study was performed to evaluate the advantages and disadvantages of both design options as detailed in Table 9.

Table 9: Fuselage Structure Trade Study

Figures of Merit	Weight	Monocoque	Semi-monocoque
Weight Efficiency	0.2	10	7
Ribbing Complexity	0.3	10	6
Manufacturability	0.1	6	8
Compatability with Doors	0.1	6	9
Structural Interface	0.1	8	9
Volume	0.2	10	6
Cost	0.1	6	9
<b>Total</b>		<b>8</b>	<b>7.55</b>

The semi-monocoque structure is easier to manufacture but lacks a larger internal volume due to the need for internal ribbing.

However, while the monocoque structure did increase the manufacturing complexity, it also increased the internal storage capacity and reduced the number of supporting parts. Therefore, the team determined that the monocoque structure was the preferred configuration for this set of rules.

### 4.2.5 Fuselage Material Investigation

As shown in Table 10, the team explored four options for the fabric for the fuselage and structure of the aircraft: fiberglass, carbon-fiber, Kevlar, and carbon-Kevlar. Since the team opted to build a monocoque fuselage as detailed in Section 4.2.4, a composite structure was needed in order to optimize strength, weight, and impact resistance. Additionally, a composite sandwich structure was utilized to allow the aircraft to be skin supported, thus validating the monocoque configuration. A structural PVC foam was selected as a core to sit between two layers (four in total) of carbon-Kevlar.

Table 10: Materials Selection

Figures of Merit	Factor	Fiberglass	Kevlar	Carbon fiber	Carbon-kevlar
Weight	0.4	5	8	8	9
Strength	0.4	6	7	8	9
Ductility	0.2	9	8	7	6
<b>Total</b>		<b>6.2</b>	<b>7.6</b>	<b>7.8</b>	<b>8.4</b>

## 4.3 Aerodynamics

The aerodynamic analysis was conducted with an amalgamation of software packages and culminated in a "proof-of-flight" Aerodynamic Prototype flight test. When determining the airfoil selection, Airfoil Tools (9) was used alongside XFOIL (10) in order to gain data regarding performance estimates. When looking at the overall configuration during the trade study phase, the aerodynamics team utilized VSPAero in order to quickly and

accurately model different aircraft variants. Static stability was hand-derived pulling from typical equations found in (1) and Dynamic Stability was analysed in AVL (11). The aerodynamics team also utilized SOLIDWORKS (12) for some quick CFD estimates for drag prediction and for a higher fidelity approach, used Ansys (13). The configuration analysis was initially tested in RealFlight 8 and was verified during a flight test.

#### 4.3.1 Airfoil Selection

When choosing the best fit airfoils, there were several factors that needed to be considered. The lift coefficient, drag coefficient, lift/drag (L/D), thickness, stall angle and stability were analyzed during the airfoil selection process. A desired airfoil for *Dragonfly* would have high lift and low drag to maximize carrying capacity and high velocity respectively. The thickness of the airfoil would affect the air flow separation: increasing the airfoil thickness would result in increasing lift. Thus, thicker airfoils were considered. The stability was analyzed by comparing moment coefficients. To establish a stable aircraft, a moment coefficient with fewer negative numbers would be suggested. In conclusion, an ideal airfoil for *Dragonfly* would be high lift, low drag, thick, and high stability.

After trade study and research, nine airfoils were selected to be analyzed and scored based on the factors listed above (see section 3.2.10). They were airfoils NACA 2412, 4412, 6412, 23012, CH10, Prandtl-D Root, Clark Y, KFM airfoil based on the NACA 0012, and NASA/Langley LS 417 Mod.

Table 11: Airfoil Data-Sheet Analysis and Downselect

Airfoil	Max C <sub>L</sub>	C <sub>D</sub> at Cruise	Cruise L/D	Cruise C <sub>M</sub>	Stall Angle	Thickness
2412	1.41	0.01	84.0	-0.05	15.3	12.0
4412	1.45	0.01	63.8	-0.10	15.3	12.0
6412	1.60	0.01	77.6	-0.14	13.5	12.0
23012	2.05	0.04	135.0	-0.22	11.0	12.8
CH10	1.21	0.01	83.7	-0.05	17.8	12.0
Prandtl-D Root	1.43	0.01	93.8	-0.09	13.5	11.7
Clark Y	1.43	0.01	67.4	-0.02	14.3	12.0
KFM	1.24	0.01	50.5	-0.05	14.8	12.0
NASA 417 MOD	1.77	0.01	54.3	-0.09	16.3	17.0

Airfoil (weightage)	Max C <sub>L</sub> (0.25)	C <sub>D</sub> at Cruise (0.4)	Stall Angle (0.15)	Thickness (0.1)	Stability (0.1)	Total Score
2412	3.09	3.11	5.00	2.82	1.12	3.16
4412	3.18	0.09	5.00	2.82	0.60	1.92
6412	3.50	1.59	5.00	2.82	0.45	2.59
23012	3.51	2.48	4.67	2.82	3.00	3.15
CH10	4.50	5.00	3.61	3.01	0.27	3.99
Prandtl-D Root	2.66	3.07	5.00	2.82	1.25	3.05
Clark Y	3.14	3.47	4.43	2.75	0.71	3.19
KFM	2.70	1.85	4.84	2.82	1.12	2.42
NASA 417 MOD	3.89	2.00	5.00	4.00	0.70	2.99

The top two airfoils appeared to be CH10 and Clark Y respectively. The CH10, as shown in the table, has the capability to provide high lift. However, the CH10 airfoil lacks stability. In comparison to the CH10, the Clark Y airfoil, is well-balanced. Additionally, the Clark Y airfoil has the capability to provide promising lift. The team decided to use the Clark Y airfoil for the front wing, and the CH10 airfoil for the rear wing. The Clark Y airfoil would be mounted at an AOA of 5 degrees, while the CH10 would be mounted at 0 degrees in the back. This

forces the Clark Y to stall at a lower AOA than the CH10 for stall recovery. Furthermore, by inclining the Clark Y at a 5 degree angle of incidence and accounting for the downwash effect, the  $C_L$  values were comparable.

### 4.3.2 Winglet Optimization

The Huskyworks team investigated winglets since these devices increase the lift generated at the wingtip while also reducing the lift-induced drag caused by wingtip vortices, improving the lift-to-drag ratio. The wingtip vortex, which rotates around from below the wing, strikes the surface of the winglet, which creates a force that reduces the rotation of the air. Even though lift-induced drag is reduced due to the implementation of winglets, parasitic drag increases as there is more surface area. There is an inverse relation where for total drag, the lift induced component is higher and the parasitic component is lower at low speeds while the opposite is true for higher speeds.

Thus, the goal is to fly the plane at relatively low speeds to gain the most use out of the winglets. When conducting the drag analysis in section 4.3.3, the team compared estimates with and without winglets as shown in Figure 10.

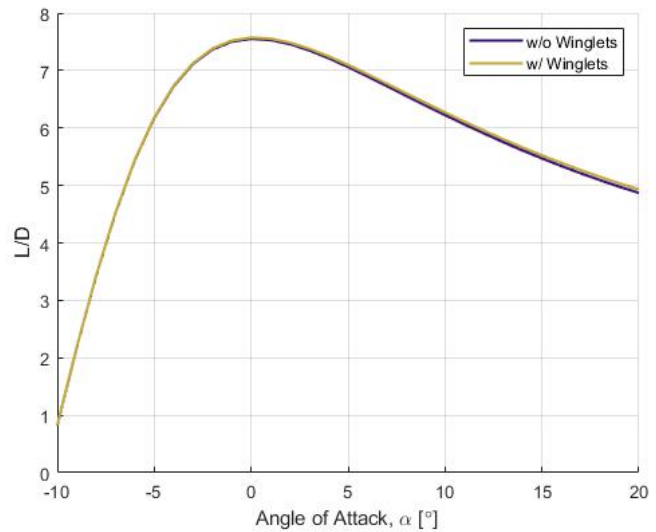


Figure 10: Effect of Winglets on L/D

### 4.3.3 Aircraft Drag Analysis

Drag data was collected from a variety of sources. Specifically, parasitic drag was calculated through VSPAero (14), induced drag through AVL (11) (AVL geometry and coefficient output shown in Figure 13), trim drag through Raymer (1), sensor drag through OpenRocket (15), and towline drag was approximated by a very small diameter 15-foot cylinder and calculated by hand. These drag forces were broken down by component in Figure 11. The primary sources of drag for all missions were the fuselage, wing, and landing gear. Furthermore, induced and trim drag vary between each of the three missions in addition to the sensor arrays' added drag in Mission 3.

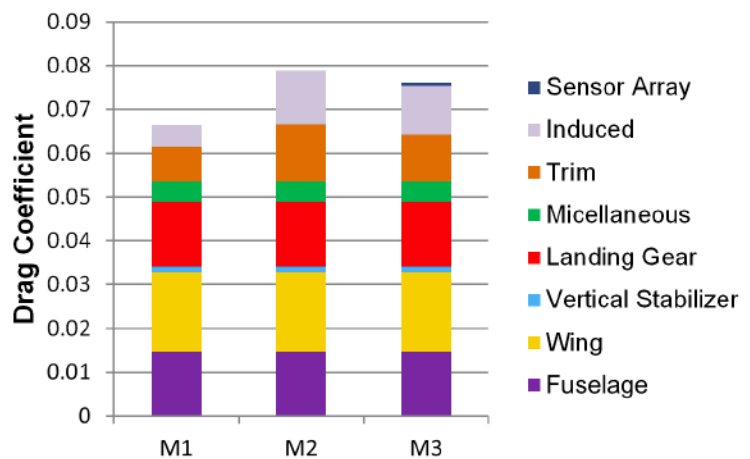


Figure 11: Breakdown of Drag Components by Mission

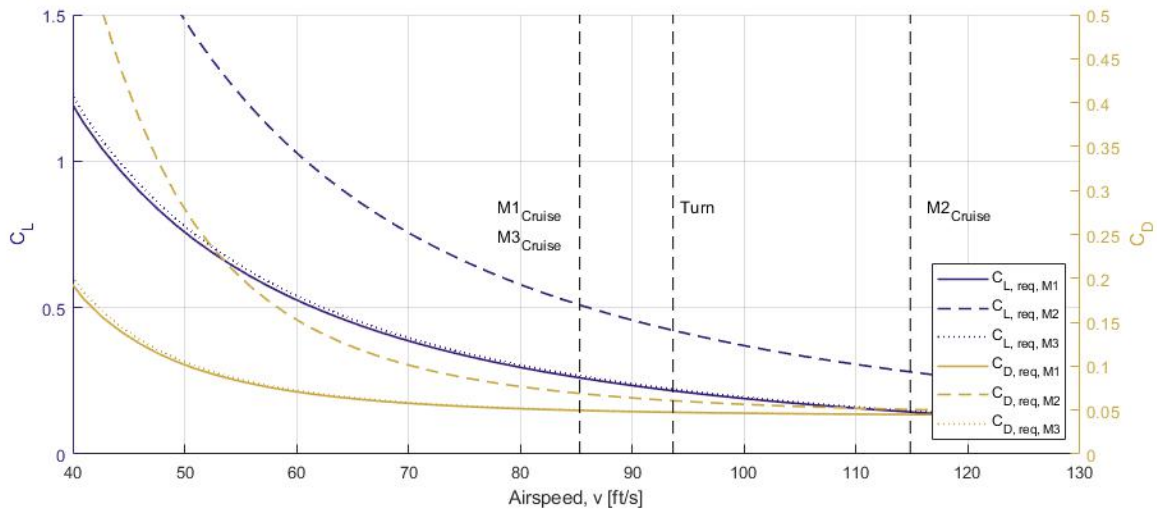
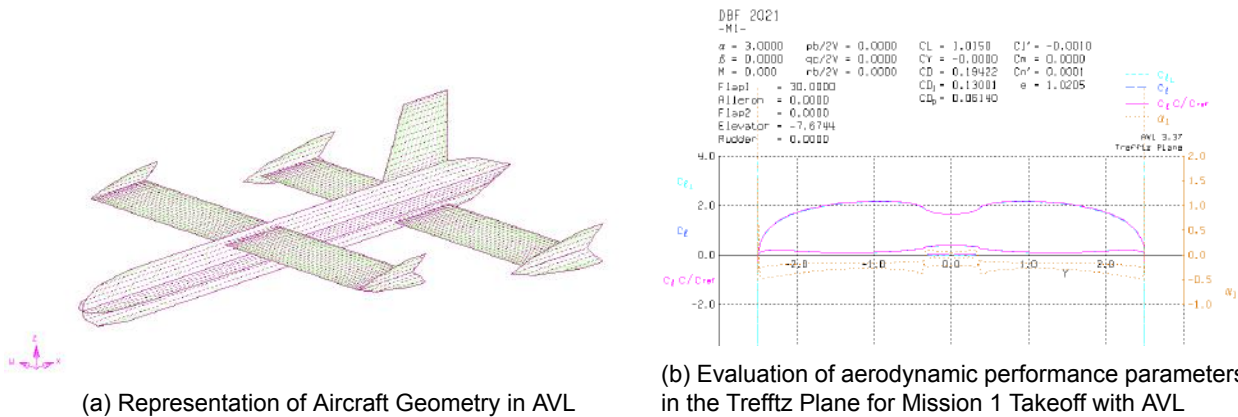


Figure 12: Dependency of Required Aircraft Lift and Produced Drag on Airspeed.

Figure 12 shows the Lift and Drag coefficients required for each mission. In Mission 2, weight increases by 18 pounds requiring more lift from the wings which increases induced drag. Trim increases to counter the larger moment the CH10 generates at a higher AOA causing trim drag to increase. This is partly offset by cruising 30% faster. Mission 3 cruise conditions are similar to Mission 1. The sensor array adds weight which requires a larger AOA and therefore increases induced and trim drag in addition to the sensor array’s own drag.



(a) Representation of Aircraft Geometry in AVL

(b) Evaluation of aerodynamic performance parameters in the Treffiz Plane for Mission 1 Takeoff with AVL

Figure 13: AVL Geometry and Performance Parameters in the Treffiz Plane

#### 4.3.4 Sensor Stability/Drag Analysis

When selecting an aerodynamic design for the sensor, the Huskyworks team took inspiration from rockets. Rockets have long been used to compactly stow a payload for precise delivery to a target. Such characteristics are ideal for the sensor design.

Table 12: Nose Cone Drag Reduction

Nose Cone	Drag (N)	Drag (lb)	Percent Difference	Surface Area (ft <sup>2</sup> )	Percent Difference
Version 1	0.076	0.017	12.921	84.4	11.863
Version 2	0.066	0.015		74.4	

Making the nose more aerodynamic had the largest effect on minimizing sensor form drag. A long elliptical nose was chosen as it has the lowest drag coefficient within the flight regime (16). Due to a rule change regarding how the sensor length was measured, the nose design was revisited to preserve the optimized length scoring. Two noses were analyzed through ANSYS Fluent: a blunted semicircular nose and the original nose. The CFD analysis showed that the blunted design decreased drag by almost the exact percentage surface area was decreased, as shown in Table 14. This similarity indicated that skin friction drag was the sensors primary drag source.

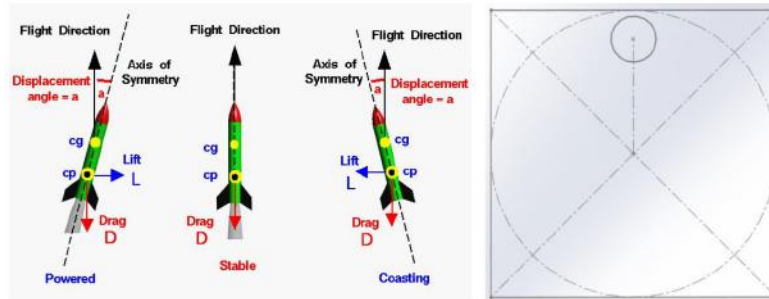


Figure 14: NASA Rocket Stability (17) and Available Area for Sensor Fins

Like a rocket, the fins are the sensors primary stabilizing device. To create a stabilising moment when the sensor is at a non-zero AOA, the CP must be behind the CG, as shown in Figure 9. In addition to flight stability, the packability of the sensor was also of great concern due to the scoring optimization. Since the sensor is circular, the fins were designed to fit into the corners of the storage box to reduce the needed space (Figure 14).



Figure 15: OpenRocket CP Prediction

Per Section 3.3.5, four fins were considered. The full body fins were insufficient at pushing the CP rearwards and thus were not considered. Testing showed that the RPG fins did not have much stability overall due to the fins small surface area. The Retractable fin design showed a high degree of stability due to its large surface area and thus was chosen during the initial analysis. In January due to AIAA rule changes, the team switched to a Conventional fixed-fin design. As these changes were made very late in the design process, OpenRocket (15) was used to rapidly evaluate several fin designs. It was found that for any given fin height, an elliptical planform fin with a root chord length of 1.22 inches was optimal for pushing the CP rearwards (Figure 15).

## 4.4 Aircraft Stability Analysis

### 4.4.1 Static Stability

Unlike conventional mono-wing designs, few guidelines exist to ensure static stability of a tandem-wing aircraft.

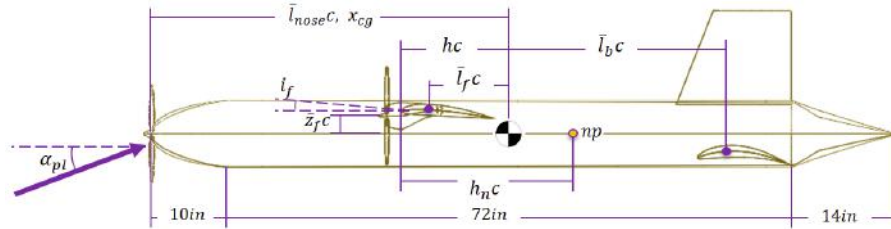


Figure 16: Geometric Dimensions Pertinent to Static Stability Analysis.

To better understand the underlying physics, Equation 12 were derived using Raymer (1) as a reference, defining the moment coefficient about the aircraft center of gravity, according to the dimensional definitions in Figure 16.

$$c_{m_{cg}} = \frac{1}{2} \cdot \{ \eta_f \cdot [c_{m_{ac,f}} + a_f \cdot \bar{l}_f \cdot (\alpha_{pl} + i + \epsilon_u - \alpha_{f_0})] + \eta_b \cdot [c_{m_{ac,b}} + a_b \cdot \bar{l}_b \cdot (\alpha_{pl} + i - \epsilon - \alpha_{b_0})] \} + \frac{m_{fuse}}{2 \cdot q_\infty \cdot S} + \frac{F_p \cdot (l_{nose} + 2 \cdot \bar{l}_f + \frac{1}{2})}{2 \cdot q_\infty \cdot S} + \frac{T \cdot \bar{z}_f}{3 \cdot q_\infty \cdot S} \quad (12)$$

Equation 12 incorporates the previously-determined tandem-wing and tri-motor geometry; the effects of propwash, downwash, upwash; and lift and moment forces. Simplifying assumptions include low AOA, small drag effects, and longitudinally-aligned PUs. From this formula, the characteristic equations for the static stability conditions of Equation 13 were defined.

$$(a) C_m \geq 0 \quad (b) \frac{dC_m}{d\alpha} < 0 \quad (13)$$

Assuming  $\Sigma T = 30$  pounds, front-rear wing incidences of  $5^\circ$  and  $0^\circ$  respectively, and rear wing placement, the condition for longitudinal static stability is summarized by the static margin's definition.

$$h_n = 0.2409 \cdot \bar{l} - \bar{l}_f - 0.02227 \geq 0 \quad (14)$$

The values for the static margin for Missions 1, 2, and 3 are 0.396, 0.362 and 0.394 respectively (per Table 15).

### 4.4.2 Dynamic Stability

The dynamic stability characteristics of the aircraft were additionally analyzed through AVL. The root locus plot of Figure 17 reveals the stability of different dynamic modes of the aircraft. Any modes with positive real parts (point of  $\sigma = \zeta\omega \geq 0$ ) are unstable.

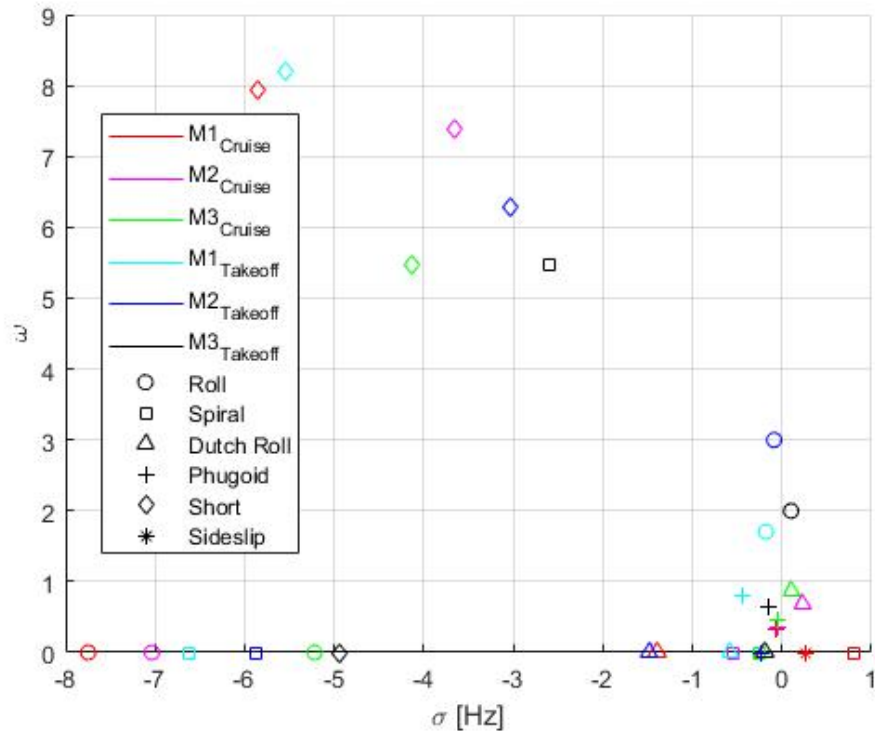


Figure 17: Eigenvalues of Stability Modes

All takeoff modes, except for Roll during Mission 3, were stable. The Dutch Roll Modes for Mission 2 and 3 cruise and the Sideslip and Spiral Modes for Mission 1 cruise were additionally unstable.

Table 13: Mission 2 Dynamic Stability Parameters (Cruise, Takeoff)

	Mode	$\zeta$ [-]	$\omega$ [rad/s]	$\zeta\omega$ [rad/s]	$\tau$ [s]
1	Roll	1.00, 0.0293	0.00, 0.4772	0.00, 0.0140	--- , 71.4
2	Spiral	1.00, 1.00	0.00, 0.00	0.00, 0.00	---
3	DutchRoll	-0.309, 1.00	0.1109, 0.00	-0.0343, 0.00	-29.15, ---
4	Phugoid	0.124, 1.00	0.0579, 0.00	0.00718, 0.00	139, ---
5	Short	0.444, 0.434	1.18, 1.00	0.524, 0.434	1.91, 2.30
6	Sideslip	1.00, ---	0.00, ---	0.00, ---	---

Table 14: Mission 3 Dynamic Stability Parameters (Cruise, Takeoff)

	Mode	$\zeta$ [-]	$\omega$ [rad/s]	$\zeta\omega$ [rad/s]	$\tau$ [s]
1	Roll	1.00, -.00758	0.0, 0.3141	0.0, 0.00238	--- , 420.0
2	Spiral	1.00, 1.00	0.00, 0.887	0.00, 0.887	--- , 1.13
3	DutchRoll	-0.114, 1.00	0.140, 0.00	-0.0160, 0.00	-62.7, ---
4	Phugoid	0.121, 0.344	0.0712, 0.136	0.00862, 0.0468	116, 21.4
5	Short	0.603, 0.546	0.870, 0.887	0.525, 0.484	1.90, 2.07

Despite the instability of these modes, the Mission 2 cruise Side and Spiral instabilities, and the Mission 3 Roll instabilities satisfied the Level 1 flight characteristic guidelines of MIL-STD-1797 (18), bringing the effects within the ability of the pilot to control. The guidelines recommend particular ranges of Mode damping ratios and Mode frequency or Mode period. These parameters for the more score-critical Mission 2 and Mission 3 are tabulated in Tables 13 and 14, respectively. It may be noted that the stable Roll Modes are far outside the suggested Level 1,  $\tau = 1.4s$  Mode period guidelines (18). This suggests that for turning flight, additional rudder actuation and increased aileron sizing will be required. This will further aggravate the Dutch Roll instabilities of the aircraft. However, discussion with the pilot concluded that the large period of the Dutch Roll Mode for all missions remains controllable. Experimental evaluation with the Aerodynamic Prototype, described in 8.1.7 confirmed this conclusion after increasing the vertical stabilizer size.

#### 4.5 Predicted Aircraft Mission Performance

The predicted aircraft performance estimates were generated using AVL and VSP Aero.

Figure 18: Performance Predictions for the *Dragonfly*

	Mission 1	Mission 2	Mission 3
<b>Weight</b>	23.3	44.78	24.3
<b>e [-]</b>	0.580	0.859	0.874
<b><math>\alpha</math> [°]</b>	-3.80	-0.64	-1.22
<b><math>\delta</math>Elevator [°]</b>	-15.90	-17.14	-15.95
<b>CL,Cruise [-]</b>	0.269	0.281	0.267
<b>CL,Max [-]</b>	1.068	1.068	1.068
<b>CD [-]</b>	0.0665	0.0789	0.0761
<b>L/D [-]</b>	4.05	3.56	3.51
<b>L/DMax [-]</b>	6.96	6.63	6.72
<b>W/S [lb/ft<sup>2</sup>]</b>	2.33	4.48	2.43
<b>vCruise [ft/s]</b>	85.31	114.84	85.31
<b>vStall [ft/s]</b>	44.29	61.40	45.23
<b>TOFL [ft]</b>	33.6	96.7	34.7
<b>Endurance [min]</b>	12.0	2.1	12.0

## 5 Detailed Design

The Detailed Design phase targets specific part design based off of the information gathered in the trade study and Preliminary Design phases. The team worked to target low-weight, high strength, and reliable components in order to maximize the efficiency of the *Dragonfly*. Part design was a largely iterative process with the prototypes fed into a series of tests in order to validate the design and final configurations.

### 5.1 Dimensional Parameters

Table 15 below lists the detailed information of different components and subsystems of the *Dragonfly*. Per competition guidelines, all avionics components are off-the-shelf. However, they are sourced specifically from the FPV Drone racing industry in an effort to bring higher efficiency components to the competition.

Table 15: Aircraft Component Summary

Front Wing		Fuselage		Motor	
Airfoil	Clark Y	Total Length	96 in	Model	iFlight XING X4214
Span	60 in	Nose length	10 in	Rated KV	660 RPM/Volt
MAC	12 in	Empennage Length	14 in	Max Power	2300 W
AR	5	Height	8.5 in	Weight	0.523 lb
Planform Area	60 in	Width	8.5 in	Internal Resistance	23.1 mOhm
Angle of Incidence	5 deg	ESC		Propulsion	
Static Margin (M1, M2, M3)	0.396, 0.362, 0.394	Model	iFlight SucceX X80A	M1	APC 13 x 10
		Rated Voltage	2-8S	M2	APC 12 x 12
Rear Wing		Continuous Current	80 A	M3	APC 14 x 12
Airfoil	CH 10	Mass	0.018 lb	Propulsion Battery	SMC Graphene V2 4500mAh 6S 40C
Span	60 in	Payload			
MAC	12 in	Sensor Diameter	1.25 in	Weight per Pack	1.30 lb
AR	5	Sensor Length	18 in	Controls	
Planform Area	60 in	Controller	Seeeduino XIAO	Controller	Matek F765
Angle of Incidence	0 deg	MOSFET	NTE2396A	Rx	Frsky RX8R Pro
Vertical Stabilizer		Lights	Vetco 10W LED	Avionics Battery	Lumenier 1300mAh 3S
Airfoil	NACA0007	Sensor Battery	GNB 300mAh 3S	Mass per Pack	0.216 lb
Vertical Span	12 in	Mass per Pack	0.10 lb	Servo	EMAX ES08MDII 12 g Metal Gear
Vertical Chord	12.375 in	Total Sensor Mass	1 lb		
Thickness	0.865 in			Winch Servo	Adafruit 360-Degree

### 5.2 Structure Characteristics and Capabilities

The aircraft structure is designed to withstand a 3g aerodynamic load with a gross weight of 45 pounds with a factor of safety of 1.5. The fuselage is designed to be a monocoque structure built of a composite sandwich of PVC foam and twill-woven carbon-Kevlar. The wing structure is composed of XPS foam and a carbon-fiber I-beam and tube, with a carbon-Kevlar skin. Two wingboxes served as the interface between the fuselage and multiple components, including the wings, main and rear landing gear, and vertical stabilizer. Motor mounts were designed for the nose and wing motors to withstand the torque and thrust generated by the motor.

## 5.3 Subsystem Design

### 5.3.1 Wing Design

The wing structure is composed of XPS foam in the shape of the airfoil and control surfaces. Carbon-Kevlar fabric is the reinforcement, and a carbon-fiber I-beam and tube are the primary and secondary spar respectively. As decided by the Aerodynamics team, the wing span is 5 feet, the chord length is 12 inches, and the fuselage diameter is 8 inches. Several calculations were performed by the Structures team to determine the structural capabilities of the wing.

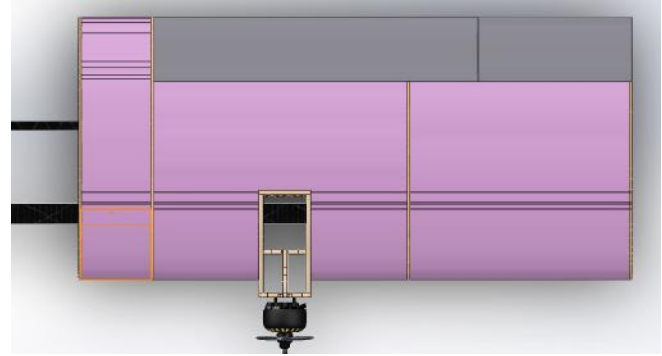


Figure 19: Internal Wing Construction

The dynamic pressure was calculated to be 0.0512 psi from the free stream velocity (945 in/s) and the air density at sea level ( $1.372 \cdot 10^{-6}$  slug/in<sup>3</sup>). Based on the wing span, chord length, and fuselage diameter, the wing area was determined to be 624 in<sup>2</sup>. The wings were built in two halves, each with a span of 26 inches. The maximum lift on each wing section is 27.8 lb (55.7 lb per wing). The maximum lift coefficient of the wing is 1.5. Assuming that the lift is uniformly distributed across the wing, the maximum bending moment at the root is 312 lb-in.

Based on manufacturer specifications (19), ignoring the web of the I-beam, the second moment of area of the I-beam cross-section is approximately 0.0142 in<sup>4</sup>. Under the assumption that the I-beam is the only bend-resisting structure in the wing, the maximum axial stress on the I-beam was calculated to be 11.9 ksi using the Euler-Bernoulli beam theory. Carbon-fiber has a tensile strength of 512 ksi and a modulus of elasticity of 33.4 msi (19). As the I-beam should have a minimum tensile strength of 128 ksi and modulus of elasticity of 8.35 msi, the factor of safety for the bending of this spar is 6.4. The wingtip deflection with the I-beam is 0.45 inches. In comparison, a circular tube of the same cross section and second moment of area of  $9.1 \cdot 10^{-3}$  in<sup>4</sup>, has 64% more deflection. Coupled with the bending and motor moment resistance, as well as the ease of wire-routing due to the channel, the I-beam was selected. A second spar was added 7 inches back from the leading edge in order to resist twisting due to aerodynamic forces. A layer of carbon-Kevlar fabric was added as a surface stiffener.

In Mission 2, the aircraft will weigh 45 pounds. The major implications of this are the need for a large amount of lift and increased roll authority due to the increased concentration of the aircraft's moment of inertia. When designing the control surface system for the *Dragonfly*, maximizing the lift and roll authority were the primary goals. Therefore, the team decided to use 87% of the front wingspan and the full rear wingspan for control surfaces. The front wings used two flaperons per wing section with an approximately 60/40 split between the inner and outer surfaces. Flaperons were used so lift could be maximised at  $C_{L,max} = 1.5$  during takeoff with maximum roll authority once in the air. For the rear wing, a more conventional elevon was chosen to counter the pitch down moment of the CH10 airfoil while further maximizing roll authority.

### 5.3.2 Fuselage Design

The inspiration behind choosing a sandwich structure monocoque composite fuselage rather than the typical semi-monocoque one was due to the need for maximum internal capacity. However, this presented an issue. By moving to a skin-supported airframe from a traditional longeron and ribbed one, there was a large risk that the required stiffness would not be achievable. Note that when referring to stiffness, this refers to the material properties that lead to the angle

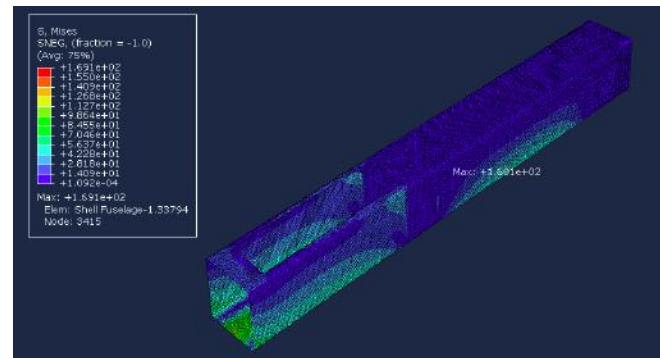


Figure 20: FEA of Monocoque Fuselage

of deflection estimate (when treating the fuselage like a beam and applying the Euler-Bernoulli beam theory). This coupled with the fact that the designed fuselage was 6 feet long meant that a lack of stiffness would lead to a lot of flex in the structure. Although a circular cross-section was the strongest, an 8-inch square with filleted corners was selected from the configuration trade study. In order to validate the proposed sandwich structure monocoque fuselage, FEA was performed, simulating competition loads.

As a note, after performing the analysis, the von Mises yield criteria was used which predicted that the maximum stress would be significantly smaller than the failure strength of the sandwich-structured composite. However, due to the uncertainties regarding the manufacturing process and concerns regarding the access hatches (large 20-inch long holes cut into the top and bottom of the structure for loading and sensor deployment), the team opted to also investigate the semi-monocoque structure as shown in Figure 21.

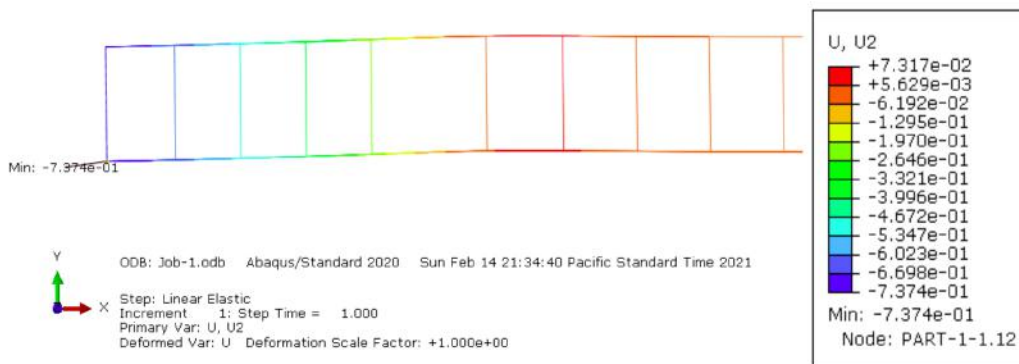


Figure 21: FEA of Semi-Monocoque Fuselage

The displacement is shown in Figure 21 and proves along with the analysis of the von Mises stress criteria that the semi-monocoque structure is also valid. However, by preparing analysis of both versions of the fuselage, the Huskyworks team was able to have a backup in case the manufacturing team was not able to create the complicated sandwich structure composite.

When the team elected to build an Aerodynamic Prototype in order to validate the stability analysis of the tandem wing design, the structures team opted to go with the semi-monocoque method for the fuselage in order to reduce cost and expedite the manufacturing process. Furthermore, since the Aerodynamic Prototype did not need to hold a high capacity of sensors, there was no need to maximize the internal capacity. However, for the Competition Prototype which was designed to take 3g turns and weigh over 40 pounds on Mission 2, the team elected to make the fuselage out of the composite sandwich structure.

The materials selected were twill-woven 5.4 oz/yd<sup>2</sup> carbon-Kevlar fabric and a scored, structural PVC foam ideal for use with a vacuum-bagging process. As shown in Figure 22, the lamination schedule determined by the team included two layers of carbon-Kevlar fabric placed so that the carbon-fiber ran along the longitudinal direction of the fuselage, leaving the Kevlar to run at a 90° angle. The twill-woven fabric would more easily conform to the complex curve of

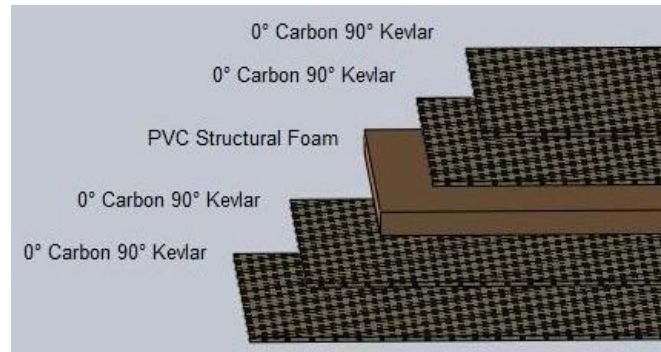


Figure 22: Fuselage Lamination Schedule

the fuselage and the carbon-fiber in the longitudinal direction meant that the structure would be very stiff. The choice to place Kevlar in the hoop direction was made in order to provide impact resistance to the composite and make it less brittle. This meant that a hard landing or a potential crash would be less likely to crack the composite frame. Between two additional layers of carbon-Kevlar the team placed a structural PVC foam to increase the thickness and stiffness.

### 5.3.3 Wingbox Design

To increase the amount of internal storage space and reduce the complexity of the composite layups, the Huskyworks team chose to manufacture the wings separately from the fuselage and mount them securely to the rest of the plane. To best use the space available within the aircraft and save weight, the structures team designed two wingboxes, one each for the front and rear wings. The technique of topology optimization (TO) was used heavily in the design of both wingboxes to improve the strength and reduce the weight of the mounts (20).

TO is a computational design strategy with the goal of producing the strongest possible shape within given constraints. TO is distinguished from other methods by its generative approach and large number of degrees of freedom. Generative design is a computational process involving a large number of iterations, organized into "generations". This process imitates evolutionary biology in choosing the highest performing iterations to reproduce, adding slight variations, and repeating this process up to several thousand generations until the optimal strength and weight is achieved. Additionally, the several million degrees of freedom involved in TO methods make such problems virtually impossible to solve analytically. Figure 23 shows the timeline of a topology optimization, (left to right) the initial bounding box, rough output, refined output, and FEA validation.

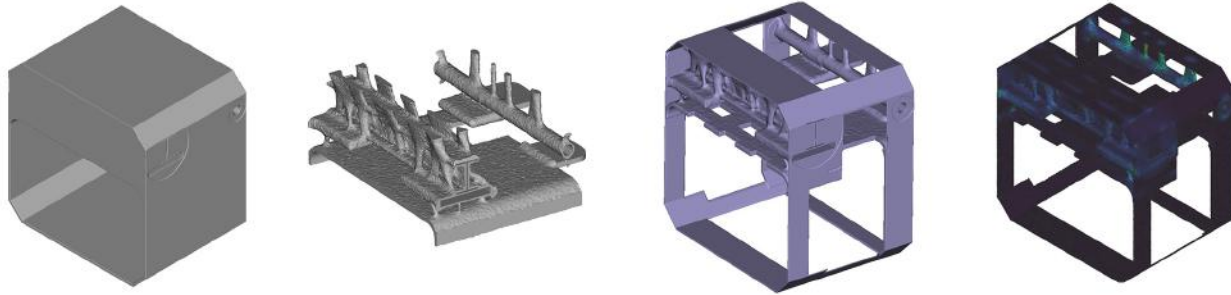


Figure 23: Visual Overview of the TO Cycle

The TO process begins by defining constraints within which the structural component must operate. A bounding box groups the first set of constraints that limits the shape and size of the final structure. This step considers the function of the part, including all surfaces with which the component interacts. The output of this step is a featureless box produced using parametric CAD. The bounding box is then imported into an optimization program, where it is split into a mesh of small elements filling the entire volume. Loading conditions, volume, symmetry, and CG constraints are defined at this point. The optimization program then begins simulating the response of the part after generating each iteration. Based on these results, material is removed from regions which do not effectively carry load and is added near regions with high predicted stress. The TO program used by the Huskyworks team, nTop Platform, uses implicit modeling to simplify the optimization by creating a density field with a domain inside of the bounding box and a range of 0 to 1. The final shape is decided by the intersection of the density field with the mesh, where only elements having an average density above a specified threshold are kept. The shape resulting from the TO process will often have sharp edges and angular protrusions; however, implicit modeling in nTop Platform greatly simplifies the refinement in two ways: the rough surface can be easily smoothed out, and the resulting body can be merged with any essential volumes that were excluded to create a functional part.

The bounding box was chosen to best fit within the composite fuselage with the intent to fasten it via adhesives. Cavities and holes were added to accommodate the spars running through the wings and electronics. A mesh with a resolution of approximately 1mm was chosen to ensure that the results would be available quickly, without sacrificing reliability. A displacement constraint of zero was applied to the faces intended to touch the fuselage skin, while the max predicted loads caused by each integrating component were applied to their respective points of contact. The rough output indicated all areas of the displacement constrained surfaces which are necessary to adhere to the fuselage, allowing for the removal of much of the surface material to reduce weight. The results of the optimization

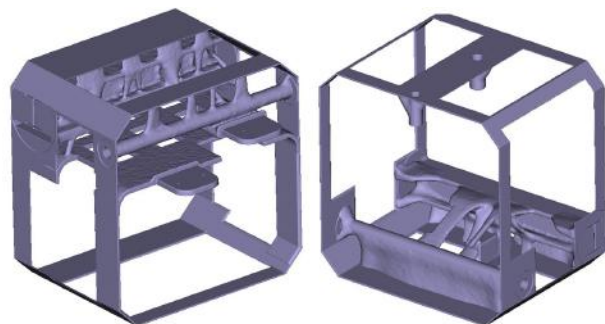


Figure 24: Selected Views of Front and Rear Wingboxes.

were validated by running the refined output through FEA.

Due to the complex geometry, 3D-printing is the only suitable method for manufacturing the wingboxes. The print orientation was chosen to minimize the effect of errors on the fit of the wing spars by placing the tubes in a vertical orientation. When the extruded filament is approximated as a fiber composite, rather than an isotropic material, this orientation also maximizes strength by placing the fibers in the approximate direction of the principal tensile stress.

### 5.3.4 Landing Gear

The team selected a taildragger configuration for the aircraft. The main landing gear was mounted to the front wingbox. An F3A style landing gear composed of unidirectional carbon-fiber core wrapped with woven cloth was purchased for this aircraft. An S-shaped, steerable taildragger was purchased and mounted to the rear wingbox.

### 5.3.5 Motor Mounts

Two motor mounts were designed: one for the nose-mounted motor and one for the two wing-mounted motors. The motors exert both a forward thrust and torque on the mounts when propelling the plane. Additionally, the motors heat up during use. Both motor mounts were designed to resist these loading conditions and minimize the effects of high temperatures.

The nose motor mount was designed to fasten to the fuselage skin via an adhesive. Sharing the goals of minimizing strength and weight with the wingboxes, the nose motor mount was optimized through the nTop Program. As the motor temperature was predicted to exceed the melting temperature of PLA, the team opted to laser cut 0.2-inch plywood and assemble the mount. The wing motor mounts were similarly designed to be laser cut and run through FEA, as shown in Figure 25.

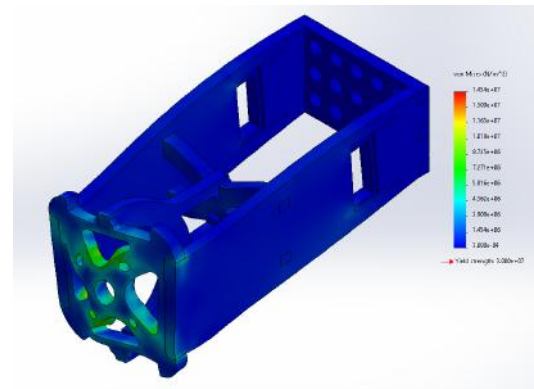


Figure 25: Wing Motor Mount FEA

### 5.3.6 Aerodynamic Cowlings

Parabolic, ogive, and cylindrical shapes were compared during the conceptualization of the nose cowling. The factors considered in this selection were drag and ambient temperature. Drag had the largest weight in this decision as the targeted mission speeds saw minimal increase in ambient temperature due to the motor. The parabolic shape was selected as it provided the most significant drag reduction. Additional cowlings were designed and 3D-printed for the wing motors and empennage. The wing motor cowlings were designed to reduce drag and slits were added to help cool the motors. The empennage was designed to be largely aerodynamic, transforming from the rounded square shape of the fuselage to a conical tip. The complex shapes of all the cowlings made them ideal for 3D-printing.

### 5.3.7 Sensor Design

To best meet the payload requirements, the Huskyworks team chose to go with a fully 3D-printed design in order to allow for rapid prototyping and ease of manufacturing. The full sensor could not be printed in one piece as it was too long for the print bed so it was broken up into a nose, fin, and individual body tube sections. Within the body tube sections, custom mounting mechanisms were designed to hold the electronics in place. An aligning steel rod goes throughout the full piece to prevent the individual sections from rotating to an unlocked position, while also resisting bending moments about the longitudinal axis.

### 5.3.8 Sensor Deployment

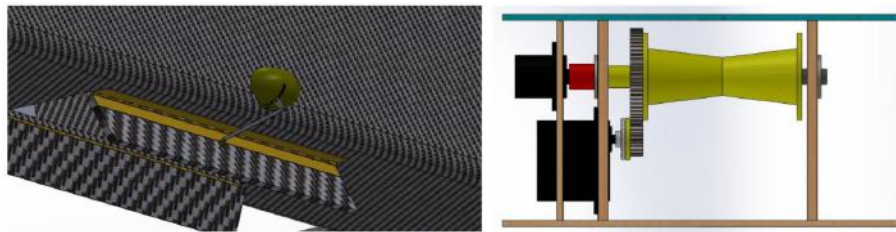


Figure 26: Bomb-bay-style Door and Winch Mechanisms.

The sensor is deployed through two bomb-bay-style hatches that lie in the middle of the fuselage. The doors are constructed out of the same composite sandwich structure as the fuselage and are attached using two 20-inch piano hinges. The doors are actuated by a pair of externally mounted servos which move a set of control rods to open and close the doors as shown in Figure 26. Once the doors are open, the sensor is deployed through the doors by a winch mechanism with a signal cable to transmit controls to the sensor. The winch itself is v-shaped to help guide the cable towards the middle of the spool. The winch is controlled by a continuous rotation servo that drives the winch shaft via a pair of gears. Signals sent from the aircraft to the sensor along the cable are transferred via a stationary slip ring and the conductive spool rod.

### 5.3.9 Sensor Storage

The sensor storage container was designed to withstand a 10 inch drop on all sides in addition to having the ability to easily load and unload a sensor. The team selected a simple friction-fit lid for the container to streamline the assembly. The container lid was designed to slide into a slot cut on the top of the container and fit snugly. The team elected to build the container out of laser-cut 0.125-inch birch wood due to the relative ease of manufacturing. A layer of 0.25-inch polyurethane foam was placed around the interior of the box to absorb the impacts sustained during the drop tests.

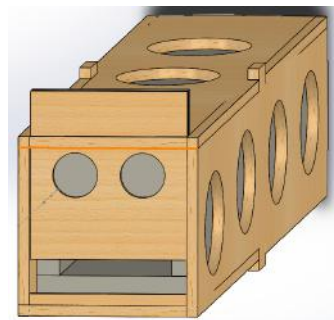


Figure 27: Sensor Storage Box Design

### 5.3.10 Avionics

The avionics system includes all electronics and components related to electronics. It is divided into two parts: aircraft circuitry and sensor sub-circuitry.

The aircraft circuitry includes the power system and flight control system. As power for propulsion consists of two parallel 6S batteries feeding three parallel PUs, a high-capacity PDB was selected to help reduce packaging size and wiring weight otherwise caused by making a complex series of Y-leads. A Matek F765 Controller was

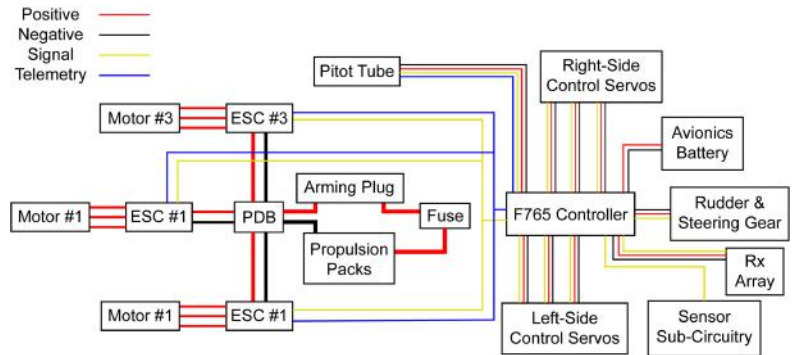


Figure 28: Wiring Diagram for Avionics and Propulsion Systems

chosen as the hub of the control circuit. Supporting digital communications, the controller decodes the signal from the RX into 12 channels of available PWM output pins. The BEC board of the F765 provides stable 5V to 7.2V power to the servos through their pin connections. Additionally, the F765 contributed significantly to the aircraft’s development as it supported black-box data recording and sensor telemetry. For the competition aircraft, in order to remove the radio frequency dead spot caused by the carbon-fiber composite fuselage, two Frsky RX8R Pro Rx were chosen to run in a redundancy series in order to improve the link to the pilot’s transmitter. To power the aircraft control circuit overall, a dedicated 3S battery powers the F765 which relays power to all control devices. This is summarized in Figure 28.

Connected to the aircraft circuitry via a signal wire between it and the F765, the sensor sub-circuitry consists of three 10-Watt LEDs, one 10-Ohm resistor, three MOSFETs, a 3S battery, and a microcontroller to control the lights. This array of components was arranged according to the circuit diagram shown in Figure 29.

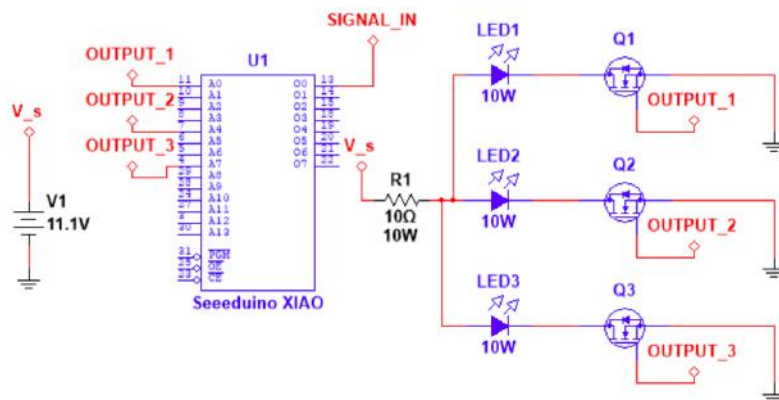


Figure 29: Wiring Diagram for the Sensor Electronics

This configuration assumes that only one of the LEDs will be turned on at a time, and that the LEDs are off by default. A “Seeeduino” (an Arduino-based third-party board) was chosen as the microcontroller since the form factor matched the sensor design. Interpreting the PWM signal from the F765, the Seeeduino controls each MOSFET to allow current through their corresponding LEDs in a programmed sequence

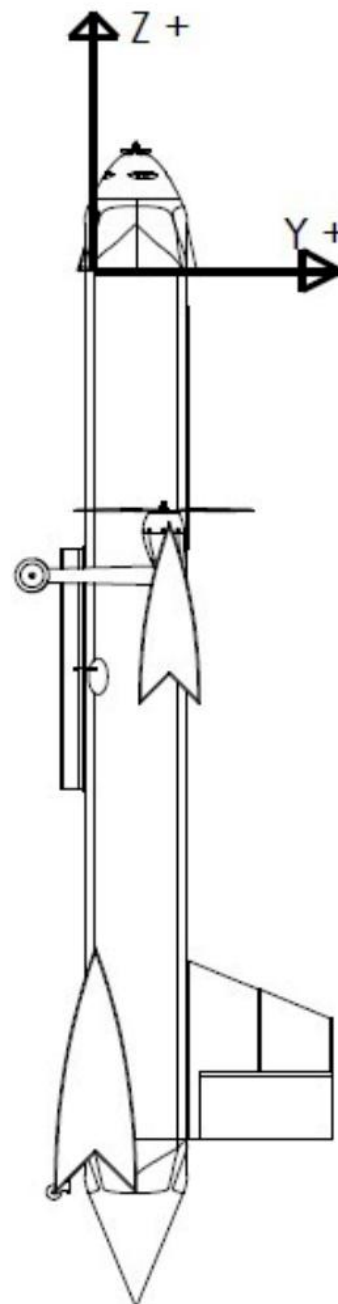
of a 1-second-on and 0.5-second-off intervals between each LED. Furthermore, the program was optimized for minimum latency and maximum responsiveness to the signal from the F765.

### 5.4 Weight and Balance

*Dragonfly's* empty weight is 23.3 pounds (10.57 kg). The two propulsion batteries and the avionics battery are contained in the nose motor mount of the plane to move the CG of the plane forward. The coordinate system used in determining the CG of the aircraft is displayed to the right of Table 16. Note that the CG is designed to fall at roughly the trailing edge of the front wing regardless of the mission.

Table 16: CG Table with Frame of Reference

Aircraft Component	Mass		Y [in]	Z [in]
	[lb]	[g]		
<b>Mission 1</b>				
Nose	0.40	182	4.26	3.50
Nose Motor Mount	1.44	654	4.25	1.50
Fuselage	5.80	2631	4.17	-37.40
Upper Acces Hatch	0.28	128	8.38	-13.00
Tail	0.44	200	13.69	-64.50
Clark Y	2.38	1079	6.48	-30.20
CH 10	2.30	1045	1.50	-68.10
Empennage	0.31	142	4.25	-76.80
Bottom Door (L)	0.20	91	0.10	-33.00
Bottom Door (R)	0.20	91	0.10	-33.00
Wing Motor (L)	0.92	417	6.55	-20.80
Wing Motor (R)	0.92	417	6.55	-20.80
Bombay Door Servos	0.06	26	1.05	-33.70
Main Landing Gear	1.46	662	-1.66	-25.70
Rear Landing Gear	0.07	33	-1.54	-74.60
Front Wingbox	0.91	413	6.19	-27.60
Rear Wingbox	0.71	321	1.28	-65.90
Front Winglets	0.24	110	7.03	-29.50
PDB	0.65	296	5.12	-15.70
AL Fuse Cover	0.45	204	4.76	-28.60
Sensor Deployment Mech	0.43	193	3.90	-31.84
Propulsion Battery 1	1.30	588	4.22	1.50
Propulsion Battery 2	1.30	588	4.22	1.50
Avionics Battery	0.13	57	0.85	-0.90
<b>Total</b>	<b>23.30</b>	<b>10565</b>	<b>4.15</b>	<b>-30.32</b>
<b>Mission 2</b>				
Forward Sensor Payload	12.89	5847	4.13	-13.70
Rear Sensor Payload	8.59	3898	4.13	-54.20
<b>Total</b>	<b>44.78</b>	<b>20311</b>	<b>4.14</b>	<b>-30.12</b>
<b>Mission 3</b>				
Stowed Sensor	1.00	454	1.54	-30.04
<b>Total</b>	<b>24.30</b>	<b>11019</b>	<b>4.04</b>	<b>-30.31</b>



## 5.5 Predicted Aircraft Flight and Mission Performance

A combination of VSPAero and AVL along with experimental data from the Aerodynamic Prototype flight test was used to determine the final predicted *Dragonfly* performance parameters shown in Table 17.

Table 17: Performance Predictions for the Competition Aircraft

	Mission 1	Mission 2	Mission 3
<b>Weight</b>	23.3	44.78	24.3
<b>e [-]</b>	0.580	0.859	0.874
<b><math>\alpha</math> [°]</b>	-3.80	-0.64	-1.22
<b><math>\delta</math>Elevator [°]</b>	-15.90	-17.14	-15.95
<b>CL,Cruise [-]</b>	0.269	0.281	0.267
<b>CL,Max [-]</b>	1.068	1.068	1.068
<b>CD [-]</b>	0.0665	0.0789	0.0761
<b>L/D [-]</b>	4.05	3.56	3.51
<b>L/DMax [-]</b>	6.96	6.63	6.72
<b>W/S [lb/ft<sup>2</sup>]</b>	2.33	4.48	2.43
<b>vCruise [ft/s]</b>	85.31	114.84	85.31
<b>vStall [ft/s]</b>	44.29	61.40	45.23
<b>TOFL [ft]</b>	33.6	96.7	34.7
<b>Endurance [min]</b>	12.0	2.1	12.0

The performance parameters were used to estimate the competition scoring results shown in Table 18. Since the *Dragonfly* was optimized for Mission 2 more so than 3, the predicted score is slightly biased towards a high Mission 2 performance.

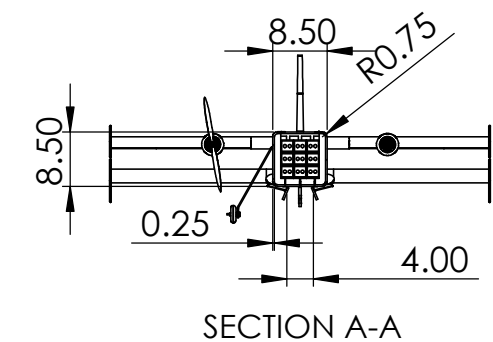
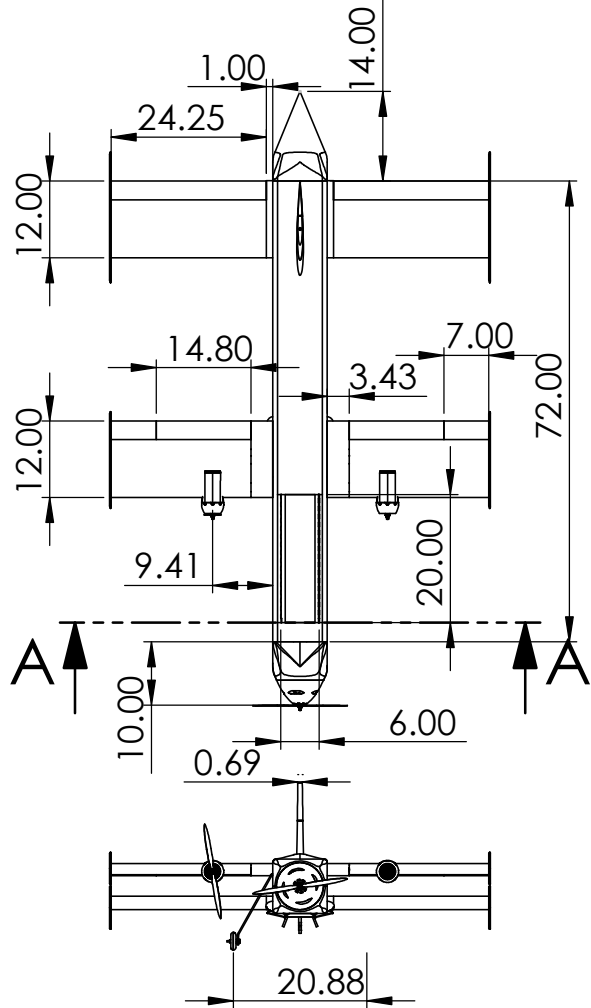
Table 18: Scoring Estimates for the Competition Aircraft

	Mission 1	Mission 2	Mission 3
<b>Completion Score</b>	1	1	2
<b>tUW [s]</b>	-	103	-
<b>tBest [s]</b>	-	60	-
<b>Nlap</b>	-	-	17
<b>Mission Score</b>	1	1.77	2.14
<b>Ground Mission</b>	0.375		
<b>Total Score</b>	5.29		

## 5.6 Drawing Package

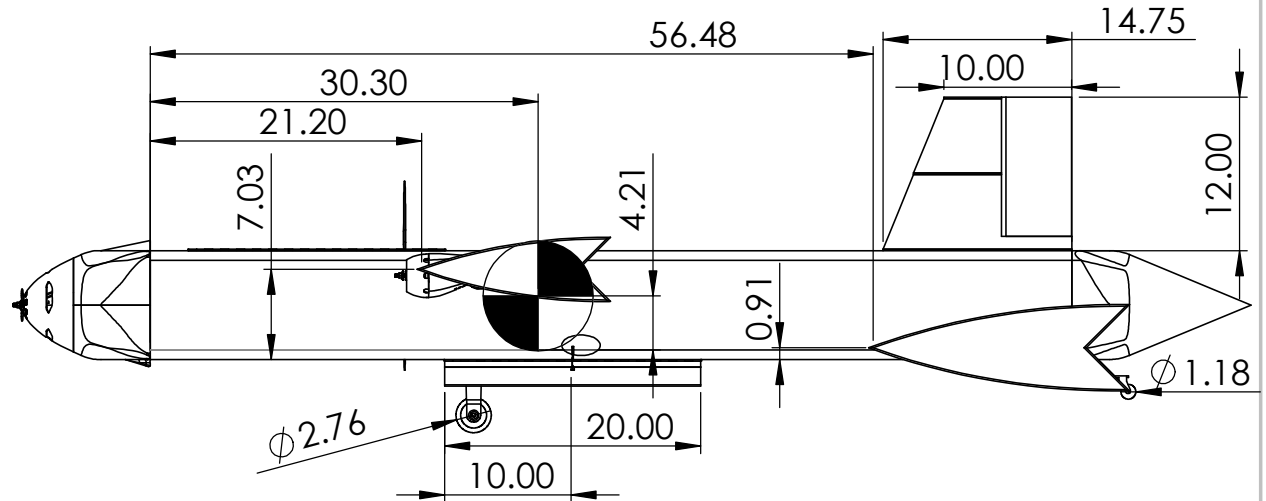
The drawing package contains a dimensioned 3-view of the aircraft, exploded views of the primary structure of the aircraft, locations of the electronics within the aircraft, and detailed views of the subsystems of the aircraft.

B

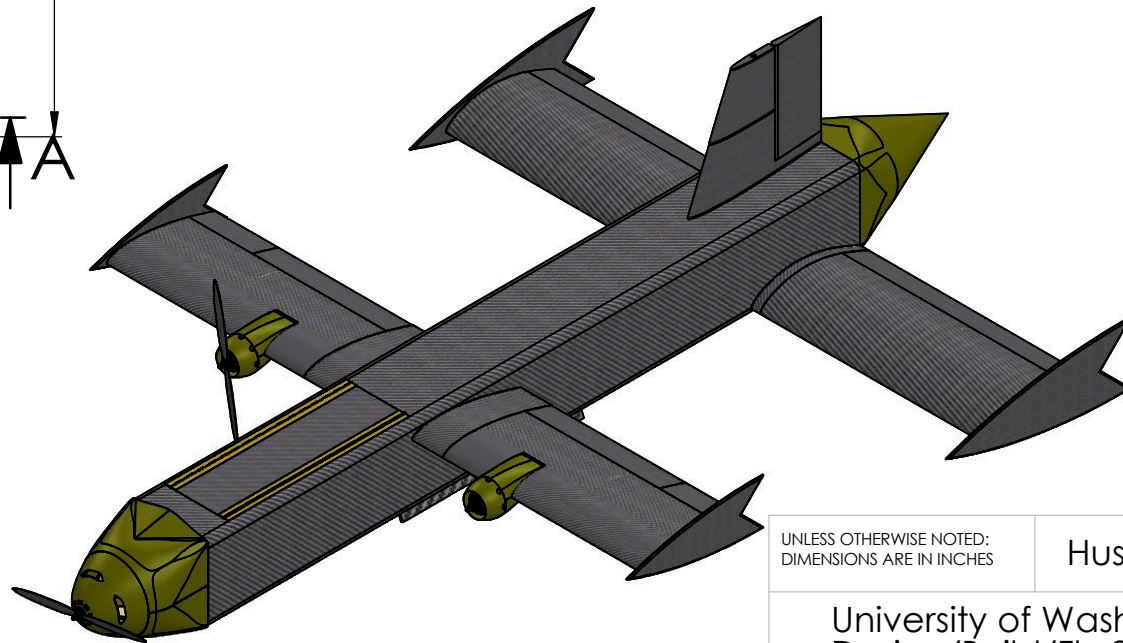


SECTION A-A

1



B



UNLESS OTHERWISE NOTED:  
DIMENSIONS ARE IN INCHES

Huskyworks

University of Washington  
Design/Build/Fly 2021

TITLE:

Dragonfly

SIZE DWG. NO.

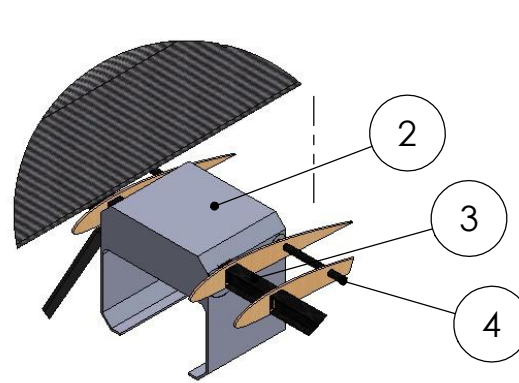
**A** Aircraft 3-View

SCALE: 1:30 Drawing Package SHEET 1 OF 4

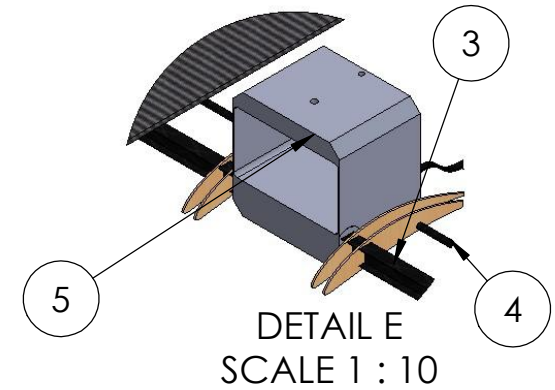
1

PART NO.	PART NAME	DESCRIPTION	QTY.
1	Nose Motor Mount	Laser Cut Plywood	1
2	Front Wing Mount	3d printed The CAD File shown is the pre-nTopology blank	1
3	Wing Spar	Carbon Fiber I Beam	2
4	Wing Spar	Carbon Fiber Rod 10 mm	2
5	Rear Wing Mount	3d printed The CAD File shown is the pre-nTopology blank	1
6	Fuselage	Carbon Kevlar composite coating over a pvc core	1
7	Front Landing Gear	Carbon Fiber Strut with 3d printed wheel	2
8	Tail Spar	Carbon Fiber Rod	2
9	Wing Motor Mount	Laser Cut plywood	2

B



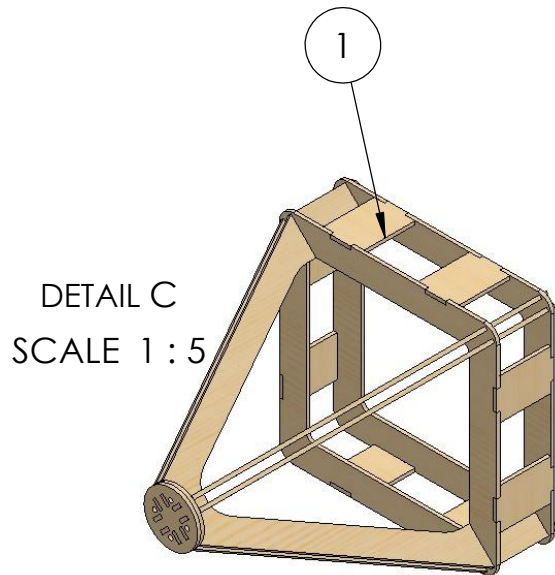
DETAIL D  
SCALE 1 : 10



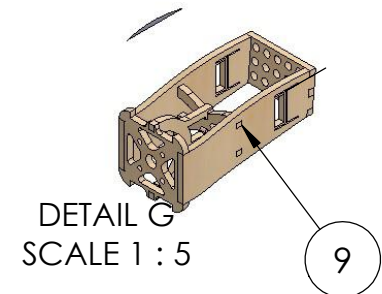
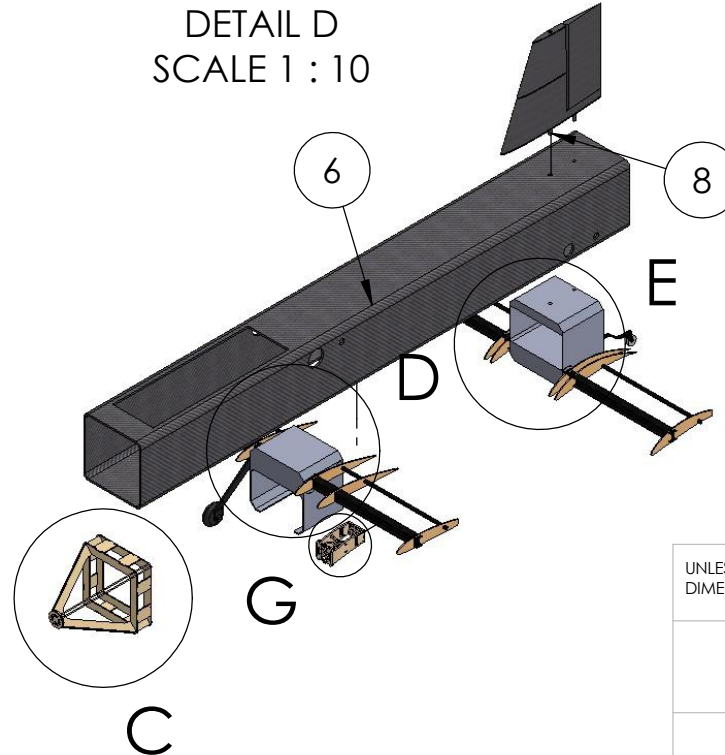
DETAIL E  
SCALE 1 : 10

B

A



DETAIL C  
SCALE 1 : 5



DETAIL G  
SCALE 1 : 5

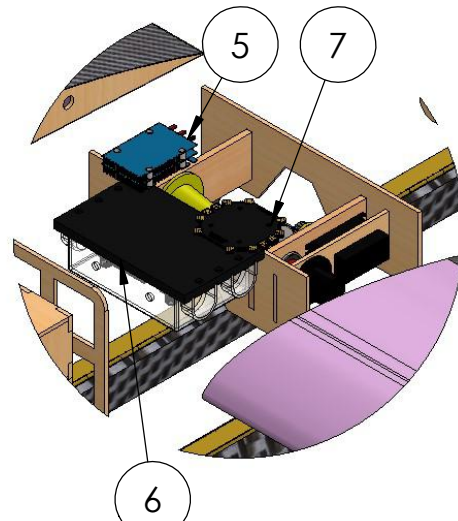
A

UNLESS OTHERWISE NOTED: DIMENSIONS ARE IN INCHES		Huskyworks
University of Washington Design/Build/Fly 2021		
TITLE: <b>Dragonfly</b>		
SIZE	DWG. NO.	
<b>A Structural View</b>		
SCALE: 1:20	Drawing Package	SHEET 2 OF 4

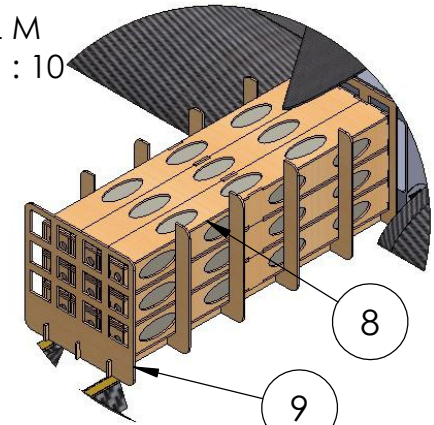
ITEM NO.	Name	Description	QTY.
1	Propulsion Battery	SMC Graphene V2 4500mAh 6S 40C	2
2	Avoincs Battery	Lumenier 1300mAh 3S	1
3	Motors	iFlight XING X4214	3
4	Esc	iFlight SucceX X80A	3
5	Flight Controller	Frsky RX8R Pro	1
6	Fuseholder	ANL Dual Fuseholder	1
7	Power Distrabution Board	APD PDB	1
8	Sensor Box	Sensor Pod storage container	18
9	Sensor Container	Laser Cut Wood Frame for sensors	2
10	Control Servos	EMAX ES08MDII 12g Metal Gear All located benneath Wing	7

B

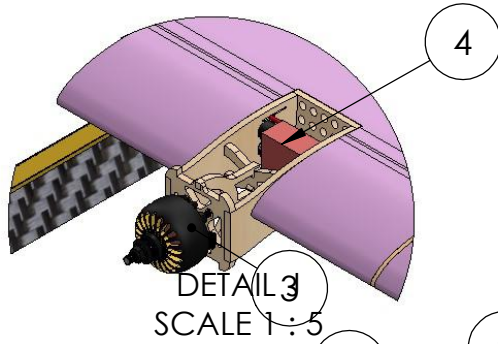
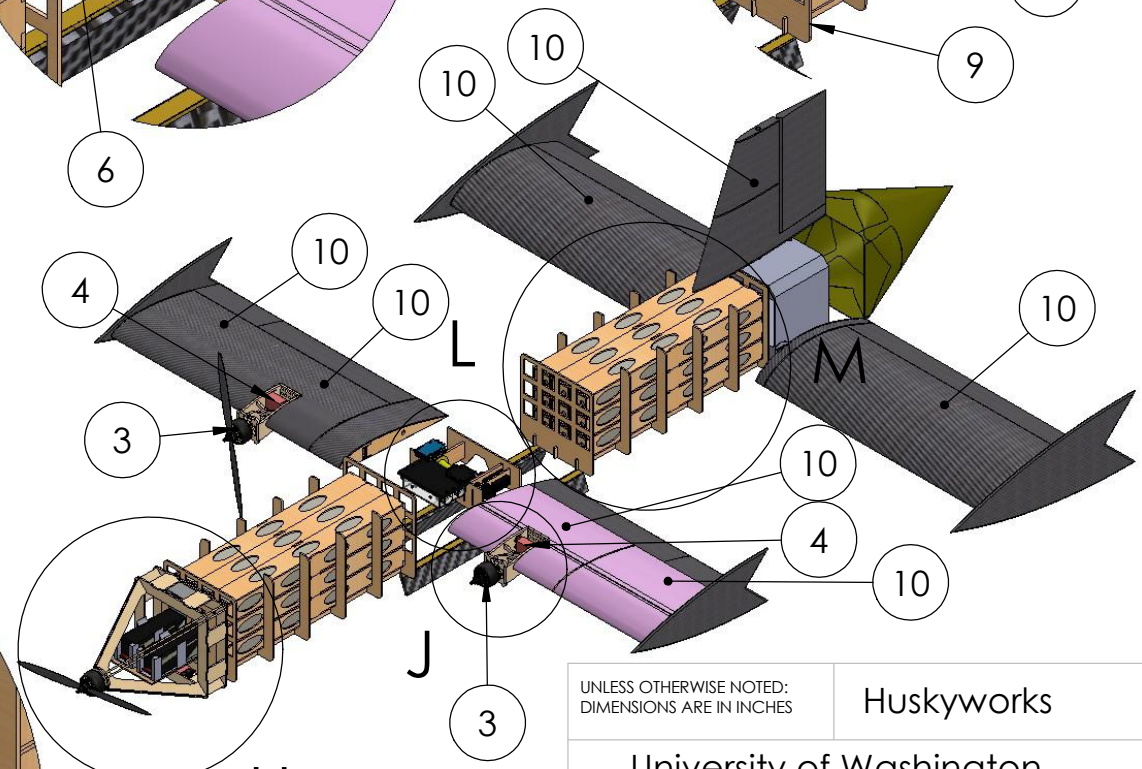
B



DETAIL M  
SCALE 1 : 10



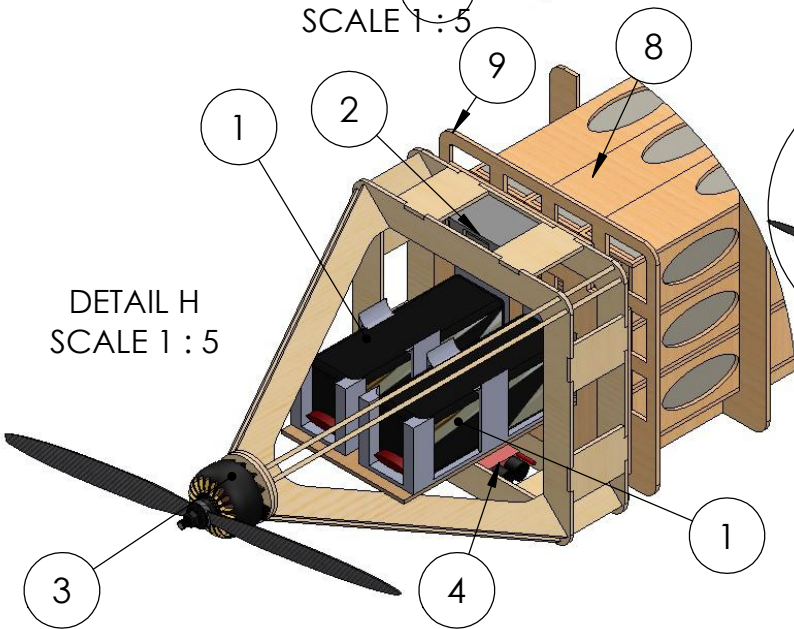
DETAIL L  
SCALE 1 : 5



DETAIL 3  
SCALE 1 : 5

A

A

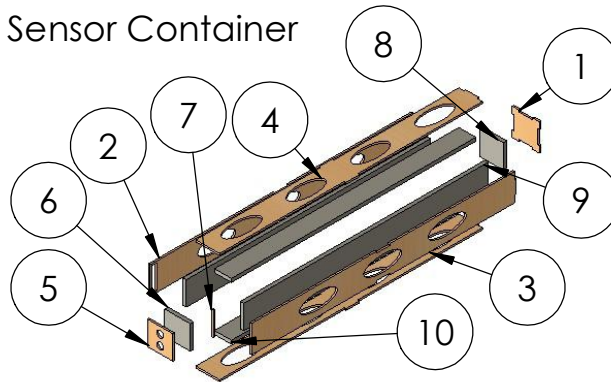


DETAIL H  
SCALE 1 : 5

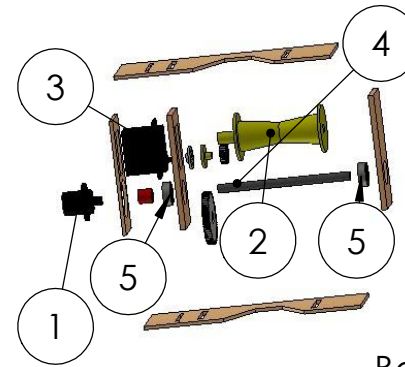
UNLESS OTHERWISE NOTED: DIMENSIONS ARE IN INCHES		Huskyworks
University of Washington Design/Build/Fly 2021		
TITLE: <b>Dragonfly</b>		
SIZE	DWG. NO.	
<b>A</b>	<b>Systems View</b>	
SCALE: 1:100 Drawing Package		SHEET 3 OF 4

ITEM NO.	PART NUMBER	DESCRIPTION	QTY.
1	Bottom	Laser Cut Wood	1
2	Side	Laser Cut Wood	1
3	Side	Laser Cut Wood	1
4	Side	Laser Cut Wood	2
5	Door	Laser Cut Wood	1
6	Door Foam	Polyurethane Foam	1
7	Door Supporter	Laser Cut Wood	1
8	Bottom Foam	Polyurethane Foam	1
9	Side Foam 1	Polyurethane Foam	2
10	Side Foam 2	Polyurethane Foam	2

Sensor Container



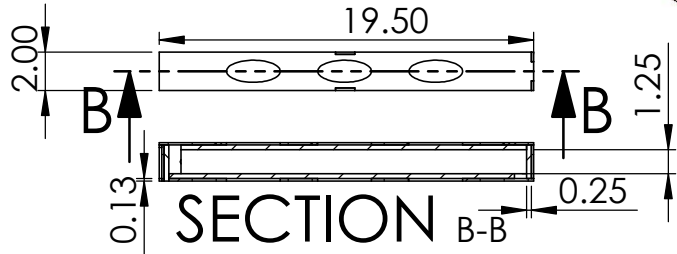
Deployment Mechanism



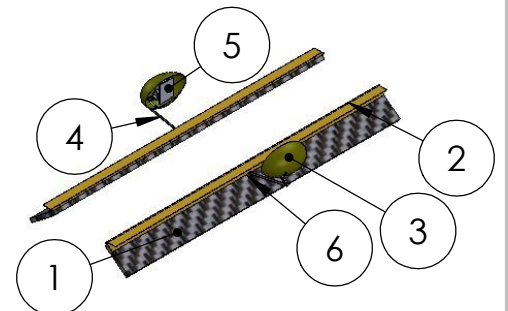
Item No.	Part Name	Description	Qty.
1	Slip Ring	Taidacent 3 wire 10 AM	1
2	Spool	3d printed	1
3	Servo	Adafruit 360-Degree	1
4	Shaft	8 mm metal shaft	1
5	Bearings	Bearing 608 2Z	1

B

B

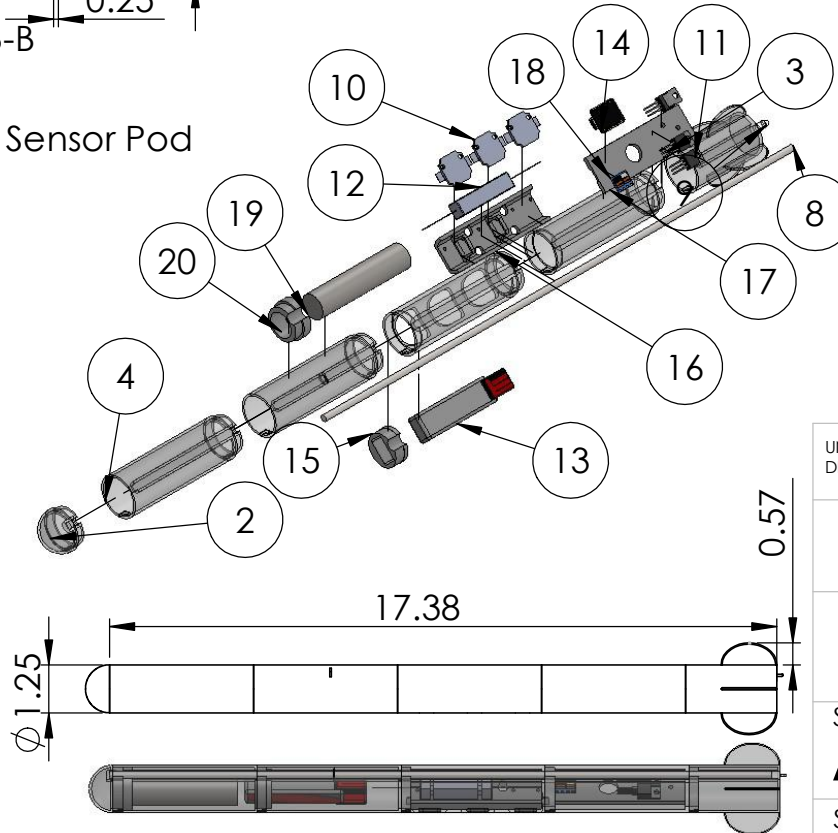


Bomb-Bay-Style Doors



ITEM NO.	PART NUMBER	DESCRIPTION	QTY.
2	Nosecone	3d printed	1
3	FinCan	3d printed	1
4	Body Section	3d printed	4
8	AlignmentRod	Steel	1
9	Cap	3d printed	1
10	LED	Vetco 10W LED	3
11	MOSFET	NTE2396A	3
12	10 Watt Resistor	CP001020R00KE 14	1
13	Sensor Battery	GN3_300mah_3 S	1
14	Microprocessor	Seeeduino XIAO	1
15	BatteryMount	3d printed	1
16	Light Mount	3d printed	1
17	Seed+MosfetMount	3d printed	1
18	Sensor BEC	lflight Micro 2-8S BEC	1
19	Steel Rod	Steel	1
20	Steel Rod Holder	3d printed	1

Sensor Pod



ITEM NO.	Part Name	Description	QTY.
1	Bomb-Bay-Style Door	Carbon Fiber Composite	2
2	Hinge	Piano Hinge	2
3	Aerodynamic Cowl	3d printed	2
4	Control Linkage	Metal Rod	2
5	Servo	EMAX ES08MDII	2
6	Control Arm	3d printed	2

A

A

UNLESS OTHERWISE NOTED: DIMENSIONS ARE IN INCHES

Huskyworks

University of Washington Design/Build/Fly 2021

TITLE:

Dragonfly

SIZE DWG. NO.

**A** Payload Details

SCALE: 1:10 Drawing Package SHEET 4 OF 4

## 6 Manufacturing Plan

When determining the manufacturing plan for the 2020-2021 year, one of the primary considerations for the Huskyworks team was equipment availability. Due to facility shutdowns and limited budget, performance versus cost analyses were key in determining the final manufacturing methods chosen below.

### 6.1 Manufacturing Processes Investigated

#### 6.1.1 Composites

Composite structures are high-cost but high-performance components because of their optimal strength-to-weight ratio. Various methods for composite manufacturing were investigated as shown in Table 19.

Table 19: Composite Manufacturing Processes Considered

					
Figures of Merit	Factor	Hand Layup	Vacuum Bagging	Resin Infusion	Autoclave
Cost	0.2	9	7	4	3
Complexity	0.2	6	7	6	3
Weight	0.4	3	5	7	9
Speed	0.2	8	7	7	5
	<b>Total</b>	<b>5.8</b>	<b>6.2</b>	<b>6</b>	<b>5.8</b>

As shown in Table 19, the composite manufacturing processes investigated were air-cured hand layups, vacuum-assisted hand layups (vacuum bagging), vacuum-assisted resin transfer molding (resin infusion), and pre-preg layups in an autoclave. These methods were compared based on cost and access to tooling, complexity, resin-to-fiber ratio achieved post-cure, and speed of manufacturing. Because the University of Washington’s Composite Shop remained closed due to COVID-19 for the 2020-2021 year, the team did not have access to an autoclave.

#### 6.1.2 Laser-Cutting

Laser-cutting allows for components to be cut very quickly and at extreme precision from thin, flat sheets of various materials. The 2-dimensional nature of laser-cutting presents some challenges, but these can be overcome by designing parts to be assembled from multiple laser-cut pieces. This process is especially useful with plywood, which can be assembled into structural components or used as stencils for cutting foam.

#### 6.1.3 3D-Printing

Since all of the component and part design is visualized in CAD software, the ability to use a CAD model to directly fabricate a part through 3D-printing allows the team to rapidly prototype and manufacture components. The major drawback is that both the strength and quality of 3D-printed structures is highly dependant on print orientation and printer quality.

#### **6.1.4 Balsa Layup**

The balsa wood layup process that was investigated follows a similar procedure to a standard wet-layup composite noted in Table 19, except it substitutes the resin for an adhesive spray. While balsa supported structures are typically weaker than composites, they can also weigh less and can be easier to manufacture.

#### **6.1.5 Covering Film**

Covering film is a type of heat-shrinkable plastic that can be molded over the top of an internal structure in order to create a lightweight and aerodynamic frame. While this method is typically weaker than the balsa layup process, it tends to also be even lighter.

#### **6.1.6 Hotwire-Cutting**

In order to create lightweight molds and structures, the hotwire-cutting of XPS foam and similar materials is often inexpensive and easy to do. Furthermore, since the process has a lower experience threshold compared to composites, it is often one of the Huskyworks team's primary methods for large part manufacturing.

#### **6.1.7 Adhesives**

Often considered a crude method of manufacturing, the primary benefit of adhesives is the ability to easily adhere parts to one another or make rapid repairs while in the field and away from more complex tooling.

#### **6.1.8 Machining**

The use of a mill or a lathe to machine parts is typically most viable for any metallic material. Machining tends to be a very high-cost and time-intensive process that outputs highly accurate (<0.005-inch tolerance) parts.

### **6.2 Processes Selected: Aerodynamic Prototype**

The primary goal of the Aerodynamic Prototype was to create an aircraft to the approximate weight and dimension of the designed CAD model. As long as the structure was sound enough to complete the Mission 1 flight, the airframe structure and materials were not of concern. Additionally, in order to have enough time to make potential design changes depending on the result of the flight test, the team also needed to be able to manufacture the aircraft quickly. Therefore, when selecting the manufacturing methods for the Aerodynamic Prototype, low-cost, high-speed, and low-complexity methods were prioritized.

The fuselage was made using a semi-monocoque method that utilized aluminum longerons and laser-cut wood ribs for the internal frame. For the skin, 0.25-inch thick hotwire-cut XPS foam was used as a skin for both the fuselage and the empennage. In addition to the laser-cut wood ribs, 3D-printed wingbox structures were used to fix the wings and the landing gear to the fuselage. The wings and vertical stabilizer were made by hotwire-cutting XPS foam and were supported by woven carbon-fiber spars. Figure 30 below showcases the semi-monocoque mainframe of the fuselage with attached wings during the XPS foam skin application process.



Figure 30: Aerodynamic Prototype Mid-Manufacturing

The landing gear selected for the Aerodynamic Prototype was identical to the one selected for the Competition Aircraft due to the need to preserve the takeoff angle so the aircraft characteristics could be properly represented. The landing gear was not made in house by the team due to complexity and instead was a purchased carbon-fiber structure. Both the main and rear landing gear are attached to the wingbox with a combination of friction clamping and bolts.

The motors were mounted by bolts onto laser-cut inserts which were built into the wing, and onto a 3D-printed structure extending forward from the fuselage. Aerodynamic cowlings were fitted over the mounts as shown in Figure 31 below in order to facilitate cooling and reduce drag. These cowlings, as they were largely non-structural, were 3D-printed out of PC (poly-carbonate) at a single shell of thickness in order to reduce weight and provide resistance to the heat generated by the motors.



Figure 31: Motor Mounts and Aerodynamic Cowlings

The Aerodynamic Prototype consisted of an aluminum and wood frame for the fuselage with additional 3D-printed supports and accessory structures. A competition equivalent propulsion system (motor, batteries, props, ESC's, etc) were used. The entire airframe was held together with a variety of common adhesives (duct-tape, scotch-tape, superglue, masking-tape, etc) due to ease of manufacturing. The aircraft weighed in at 18.5 pounds and was an accurate representation of the desired design. While the final aircraft shown in Figure 32 below may not have met the conventional aesthetic of an aircraft, it was nonetheless well built and fully functional.



Figure 32: Final Aerodynamic Prototype (Post-Flight Test)

### 6.3 Processes Selected: Competition Aircraft

The methods selected to build the competition aircraft differed from those selected for the Aerodynamic Prototype since the airframe needed to be sound enough to sustain higher loads for Mission 2 and 3. While some manufacturing methods remained the same, the main difference was the move to a 90-percent composite, skin-supported airframe. Therefore, the manufacturing methods chosen to build the competition aircraft were a combination of composites, 3D-printing, laser-cutting, and hotwire-cutting.

#### 6.3.1 Fuselage

The fuselage was manufactured in two halves. A female mold was constructed using particle board and 3D-printed fillets. Nylon release film was placed into the mold so that the part could be released from the mold post-cure. The constructed mold and combined fuselage halves are shown in Figure 33.

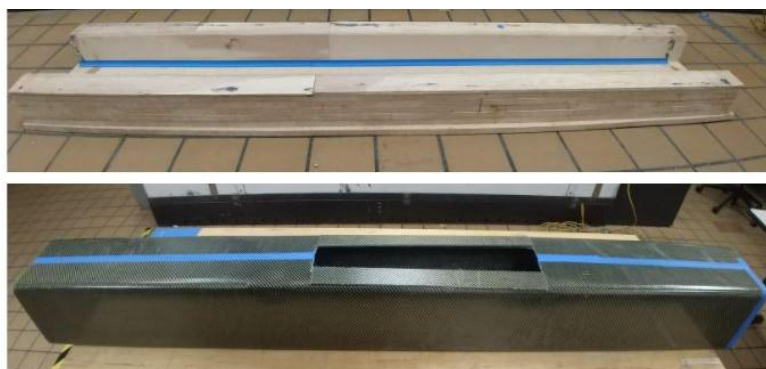


Figure 33: Fuselage Mold and Structure

A hand layup was performed following the predetermined lamination schedule as shown in Figure 22. One layer of perforated release film was placed on the wet-layup composite to finish the surface and allow resin to flow

through. A layer of breather cloth was added to absorb the excess resin. The vacuum bag was sealed around the mold. Pleats were created in 10-inch increments to increase the surface area of the bag to prevent tears. Each half of the fuselage was left to cure under elevated pressure for 12 hours. Post-cure, the two halves of the fuselage were cut and joined around the 3D-printed wingboxes using epoxy and tape as shown in Figure 33. Holes were cut on the top and bottom of the fuselage for accessing sensors and electronics and deploying a sensor. The bomb-bay doors were secured to the mainframe using a piano hinge and are operated by servos during Mission 3.

### 6.3.2 Wings

The two wings were built using a combination of hotwire-cutting, laser-cutting, and composite layups. Airfoil stencils were laser-cut out of wood and were hot-glued onto foam blocks. The wing planform was cut using a hotwire and sanded until smooth. On the front wings, a bandsaw-style hotwire-cutter was used to cut holes for the motor mounts. Wood ribs were laser-cut and hot-glued into the wings to provide structural points for the spars.



Figure 34: Wings Before and After Composite Layup

One layer of carbon-Kevlar fabric was wet-laid onto the foam wing. Due to the placement of a structural I-beam within the foam-core wing, the team chose to build the wings using an air-cured wet-layup rather than a vacuum assisted wet-layup to maintain the integrity of the I-beam channel. Release film was laid on top of the curing composite to produce a finished surface. The wing was sanded post-cure, and control surfaces were re-attached using a strip of Kevlar.

### 6.3.3 Compatible Components

The manufacturing procedure for several components of the Aerodynamic Prototype were only slightly modified for the Competition Aircraft. The process for building the wing motor mounts and wingboxes remained the same, accounting only for the change in wing structure from the traditional circular spar to a carbon-fiber I-beam. The same nose and wing motor cowlings were replicated for the competition aircraft. Additionally, the same landing gear was purchased and used in the competition aircraft. To streamline manufacturing, the team decided that the empennage would be 3D-printed. The nose motor mount was laser-cut as opposed to 3D-printed in order to save weight, however the shape remained unchanged.

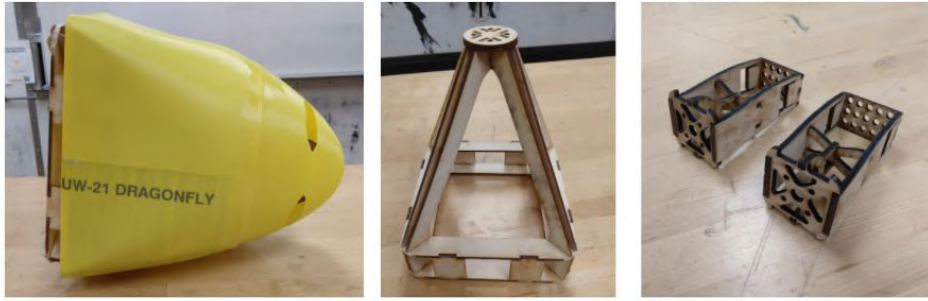


Figure 35: Nose Cowling and Motor Mounts

#### 6.3.4 Sensor

The sensor was 3D-printed using PLA in multiple parts and assembled using the included twist-lock mechanism and the aligning steel rod. 3D-printing the sensor allowed the team to test multiple fin designs, as the design could easily be adjusted and re-printed. The sensor was towed using braided fishing line rated for 100 pounds. The wire controlling the sensor was braided around fishing line, leaving slack in the wire so that the fishing line takes most of the load ensuring the wire will not break when deployed. For the sensor deployment mechanism, the tow cable was wrapped around a spool attached to a 360-degree servo. This mechanism was secured to the front wingbox directly above the bomb-bay doors.

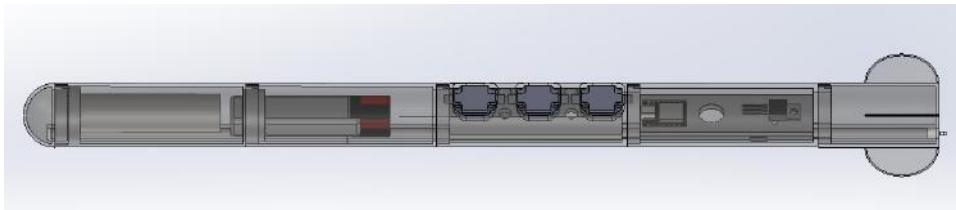


Figure 36: Sensor Internal and Configuration View

#### 6.3.5 Sensor Storage Container

Two types of boxes were constructed to hold sensors. Three containers were built to carry the real sensor and withstand a 10 inch drop. The remaining containers were built to replicate the size, weight, and CG of the real container. The materials selected for the real sensor container were selected based on the ability to survive a 10-inch drop. It was decided to laser-cut 0.125-inch birch plywood to provide a rigid structure for the container. 0.25-inch polyurethane foam lined the internal surface of the container to provide impact resistance. XPS foam was cut and sanded to shape for the remaining sensor containers. A hole was drilled into the center of each container and a steel rod was inserted to replicate the weight of the actual sensor.



## 7 Test Plan

Since facility and resource access during the fall and winter quarters was limited due to COVID-19 restrictions, the Huskyworks team worked to re-design the test plan in order to narrow down the test requirements to only the most essential systems. To do this, the team outlined the test matrix shown in Figure 38. There were four verification and validation (V&V) techniques proposed: Inspection, Analysis, Demonstration, and Test. These classifications were taken directly from a Boeing SOP for testing during a project advisory meeting. The primary distinction was that the Test technique required a lengthy setup, documentation, and analysis process while the other techniques could be done much more efficiently. The goal was to validate as many systems without a full-fledged test as possible in order to reduce the resource and expense strain on the team.

Component/System	Component Level	Design V&V	Mfg. V&V	System V&V
<b>Aircraft: Aerodynamic Prototype (AP)</b>	1	A	I/D	T
AP Fuselage	2	A	I	D
AP Wing	2	A	T	D
AP/CP Propulsion System	3	A	I	T
AP/CP Actuators	3	I	D	D
AP/CP Landing Gear	2	I	I	D
AP/CP Vertical Stabilizer	2	A	I/D	D
AP/CP Wing Box	2	A	I	D
<b>Aircraft: Competition Prototype (CP)</b>	1	D	D	T
CP Fuselage	2	A	D	D
CP Wing	2	A	D	D
<b>Aircraft: Competition Aircraft (CA)</b>	1	D	D	T
CA Max Payload Configuration	2	A	D	T
CA Sensor Storage Box (structure)	3	A	D	D
CA Sensor Deployment	3	A	D	T
CA Sensor Stability	3	A	D	T
CA Sensor Operation	3	A	D	D

Figure 38: Test Classification Matrix

The main requirements of the test matrix was that every "component level 1" system must be validated by a Test. Additionally, every system must be validated by either a Demonstration or a Test. These two stipulations ensured that the Huskyworks team had physical proof of operation for each designated system.

### 7.1 Test Schedule

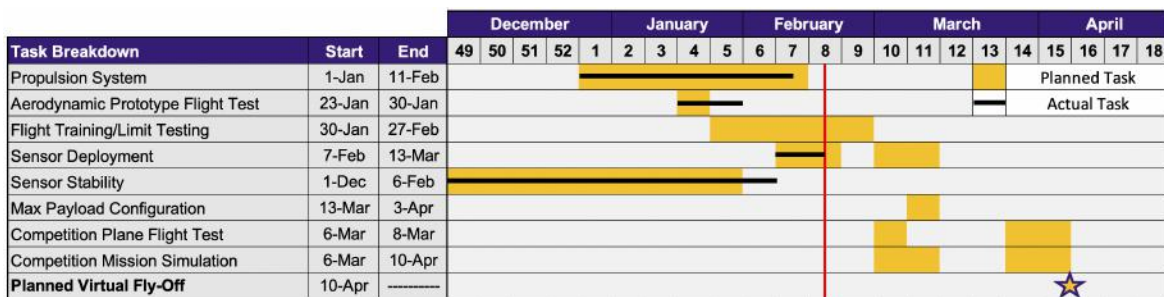


Figure 39: Test Schedule

The test schedule shown in Figure 39 outlines the plan for each of the designated Tests identified in Figure 38. In order to optimize testing while balancing the need to design and manufacture, the team tried to create a system where only one major test was run at any given time. As of February 19<sup>th</sup>, the Huskyworks team has completed all critical tests except the *Max Payload Configuration* and the *Competition Mission Simulation* flight with the final competition version of *Dragonfly*.

## 7.2 Testing Objectives

The following list is a breakdown of the test objectives noted in Figures 38 and 39 and subsystem requirements.

### Aerodynamics

- The *Aerodynamic Plane Flight Test* was tasked with validating the results of the static stability analysis in lieu of a wind tunnel test.
  - Pilot feedback coupled with on-board black box data from the flight controller was used to verify airspeed, stability, and maneuverability.
- The *Flight Testing/Limit Testing* phase will verify the performance limits (TOFL, endurance,  $v_{cruise}$ ,  $v_{stall}$ , etc.) of the *Dragonfly* and its propulsion system.

### Structures

- Cantilever, point-load beam tests, and structural demonstrations were used to validate the results of the FEA of the fuselage, wing, and relevant internal mounts.
- A pre-flight wingtip test was used to verify the airframe structure and simulate technical inspection.
- The *Flight Testing/Limit Testing* phase will verify the structural limits of the aircraft during high-g maneuvers, takeoff, and landing.

### Propulsion/Avionics

- A static thrust test was used to verify and finalize the results of propulsion sizing from the preliminary design phase.
  - A load cell coupled with a voltage divider and ammeter were used to record thrust, voltage, and amp draw in order to calculate max thrust and endurance.
- A pre-flight control system demonstration verified controllability and simulated technical inspection.

### Payload

- The *Sensor Stability* test was used to validate the CFD analysis on the stability profile of the fins and body.
  - Flight testing consisted of attaching the sensor to a quadcopter drone and simulating mission laps while recording visual data from the ground and on-board the drone.
- The *Sensor Deployment* test was used to verify the rotary deployment mechanism on the *Dragonfly*.
- The *Max Payload Configuration* flight test will verify the performance of the aircraft at max GTOW.

## 7.3 System Testing

### 7.3.1 Thrust Stand Motor Test

In order to validate the results of the preliminary propulsion sizing (section 4.2.4), the thrust test was designed to evaluate the three motor options and determine which was best for the *Dragonfly* in three stages.

In the first stage, the candidate motors were run on the same heavy-loading prop for a max thrust test to determine which motor had the greatest "potential" to do work. This measured thrust was termed "potential" because the motor's ability to produce thrust and speed depended on the design of the prop. Figure 40 indicates the correlation between a motor of a fixed potential and props of the same diameter but different pitch. A heavy-loading prop was used for testing since it normalized the load and enabled comparison for the maximum performance of the selected motors.

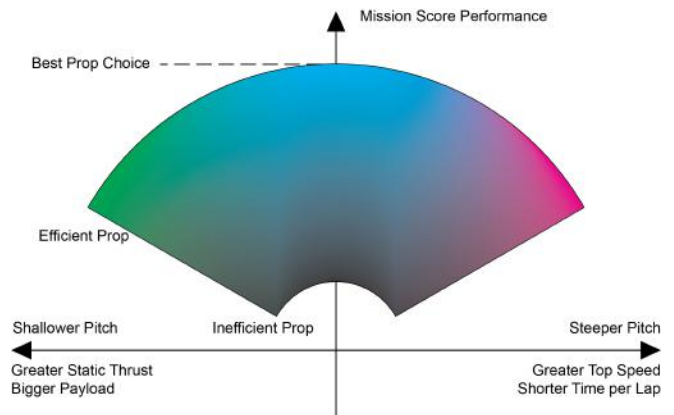


Figure 40: Correlation between Performance and Prop Choice

In the second stage, the top two performing motors were run on a 12 x 12 prop to measure both thrust and current draw during Mission 2. As long as the measured current draw stayed under the power limits established under section 4.2.4, the motor with the greater thrust was chosen. In the third stage, the final motor was run on different props to study correlations between prop speed, power draw, and thrust. The data from this section of the test helped determine the final prop choice. All three of the motor tests were run on a custom designed thrust stand shown in Figure 41. The stand could measure voltage, current, and thrust which allowed the team to gain significant insight into performance and ultimate sizing needs.

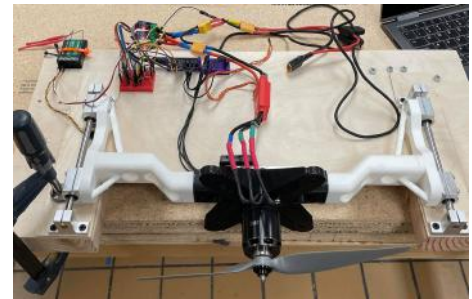


Figure 41: Thrust Stand Setup

### 7.3.2 Structural Testing

A structural wing test was performed by the team over the summer of 2019 (21). This evaluated the strength of six different composites through a Cantilever beam test. The team built a wing vice from laser-cut wood and epoxy which extended 18 inches of a control airfoil over the edge of the table as shown in Figure 42. Five XPS core composite wings were made with a combination of 1/32-inch balsa wood, 0.75-oz/yd<sup>2</sup> fiberglass, and 9-oz/yd<sup>2</sup> fiberglass chopped strand mat. Additionally, the team tested a wing made just from foam as a control variable and an experimental wing made from birch wood ribbing and covering film. Weight was then added to the tip of the wing under the assumption that if the wing could withstand a point load at the tip of the wing, it can withstand the same load as a distributed force over the surface area of the wing. The angle of deformation and

surface deformation were recorded. These results were used to determine stiffness. The team replicated this test for the materials chosen for the 2021 *Dragonfly*, XPS foam and carbon-Kevlar fabric, and compared them to the historical data to determine the best material to use. As a note, in addition to the Cantilever beam test, a wing tip test was performed on the Aerodynamic Prototype to verify wing strength. Prior to flight, the Competition Aircraft will be subjected to the same test.

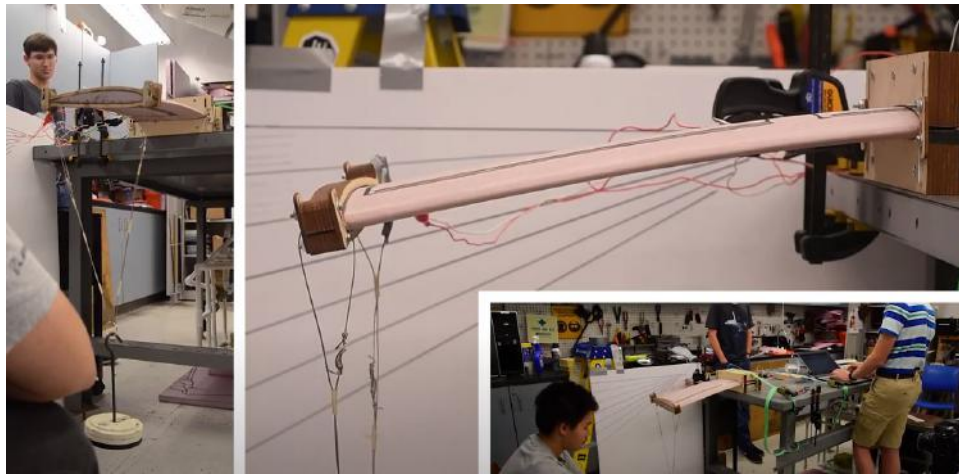


Figure 42: Cantilever Beam Test Setup

### 7.3.3 Sensor Stability

During Mission 3, the sensor must neither roll nor spin while being deployed, operated, and recovered by the aircraft. A flight test was conducted to qualitatively demonstrate roll, pitch, and yaw stability. The sensor was tethered to a quadcopter via a 15-foot tow cable and flown at Mission 3 speed. The tow cable was mounted to the CG of the sensor and the sensor body was loaded with steel rods to simulate the weight of the payload and avionics. High speed linear and curvilinear flight paths were conducted to simulate competition maneuvers. A wide angle video camera on the quadcopter and a camera on the ground recorded the flights. Visual feedback from the video recordings and from team members on the ground was used to verify the stability of the sensor fin and body configuration.

### 7.3.4 Sensor Deployment

To complete Mission 3, the sensor needs to leave the aircraft via the aircraft's bottom doors, extend to a length of 10 times that of the sensor, and retract back into the aircraft. To test this, the aircraft will be set up on a pair of tables with the doors unobstructed. The aircraft will then be turned on with the receiver connected and the doors will be actuated open to verify their function. The sensor will then be dropped out of the aircraft with the winch unwinding the cable until it has fully deployed. The retraction process will then begin, winding the cable back around the winch bringing the sensor back into the fuselage. This test will be done during a later flight test as well to verify the functionality while in flight.

### 7.3.5 Sensor Operation

The test for the electronics consisted of three stages: testing whether a PWM signal required connection to a common ground, testing the timing of the Arduino code, and testing relays to control high-power LEDs. The PWM test setup was simple. Two Arduino boards were necessary, with the output of one connected to the input of the other. One board sent a PWM signal to the other board without the boards being connected to a common ground, alternating from high to low every second. The second board then controlled an LED based on the input, so if the second board sensed a change in input, it turned on the LED. If the LED turns on, it proves that there does not need to be a common ground between boards, and there will only need to be one connection between the body of the plane and the sensor, instead of two.

The second stage of testing was slightly more involved. The necessary code was uploaded to the Arduino, then three small 2.2 V red LEDs were connected in the configuration shown in Figure 43. If the code works properly, the LEDs should turn on and alternate once every second. The third stage of testing with the high-powered LED required an alternate power supply, like the one that will be used in the sensor, as the Arduino will overheat if 10 Watts of power continuously run through it.

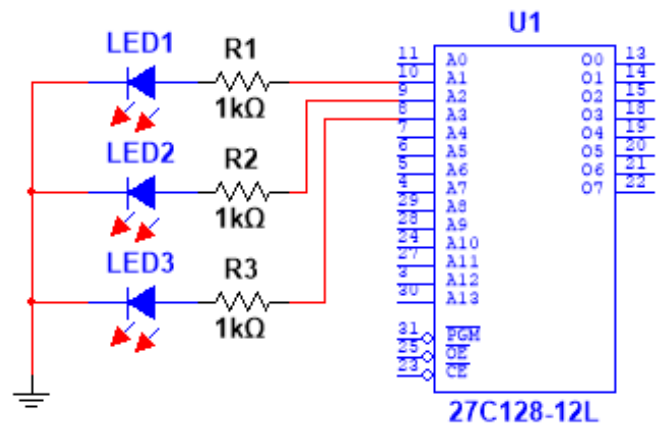


Figure 43: Circuit Diagrams for the Timing Test

### 7.3.6 Sensor Container Drop

During competition, the sensor must withstand a 10-inch drop within the sensor container. In order to test the structural strength of the sensor and container, one container was constructed and loaded with a sensor. This was then dropped from a height of 10 inches on all six faces of the box. The box and sensor were examined before and after the drop test to determine if container provided sufficient protection.

### 7.3.7 Aerodynamic Prototype Flight Test

The Huskyworks team chose to verify the predicted aerodynamic characteristics of the design by constructing a full scale prototype out of cheap, easily repaired materials that was capable of completing Mission 1. This allowed the team to conduct flight tests which provided information on the stability of the design, as well as gave the pilot more experience. The results of these flight tests were recorded in video in the air by a quadcopter and by team members on the ground. The video footage was analyzed by the pilot and observers to document the characteristics of the design. The goal of these tests was for the pilot to determine the responsiveness, stability, and handling of the aircraft while in flight. The results of these tests would assist the team in adjusting minor components of the aircraft design, such as the vertical stabilizer and control surfaces.

## 7.4 Flight Test Schedule and Plan

Flight tests were an integral part of tangibly verifying the design, especially due to the tandem wing configuration. This configuration's experimental nature required additional flight tests using a prototype aircraft, each with specific objectives. Table 20 specifies the model used and the exact objectives to be met. If the objectives of a flight test are not met, the test will be re-conducted during the next available window to ensure the program remains on schedule. It should be noted that the tests from February 20<sup>th</sup> onward are scheduled for the future.

Table 20: Flight Test Schedule

Date	Equipment	Objectives
Jan 23, 2021	Aerodynamic Prototype	Demonstrate design flight capability with full-scale, easily repaired foam prototype and trim aircraft (Result: yaw instability, crash, and vertical tail redesign)
Jan 30, 2021	Aerodynamic Prototype	Demonstrate design flight capability with full-scale foam prototype and trim aircraft (Result: stable flight achieved, one lap completed)
Feb 20, 2021 Feb 27, 2021	Aerodynamic Prototype	Explore flight envelope of the foam prototype (turns, slow flight, stall, high-speed, landing). Allow pilot to become familiar with handling. Rig a sensor to the aircraft to test its stability combined with the aircraft.
Mar 6, 2021	Competition Aircraft	Trim composite aircraft, verify handles like the prototype. Deploy and retract sensor to test and refine mechanism. Simulate Mission 3.
Mar 13, 2021	Competition Aircraft	Demonstrate refined sensor deployment if necessary. Demonstrate flight with varying payloads. Simulate Mission 2.
Apr 10, 2021	Competition Aircraft	Simulate all competition missions.

## 7.5 Flight Checklist

A standardized flight checklist was created for all test flights to ensure crew safety, proper data collection, and efficient use of pre-flight preparation time. The checklist is shown in Table 21. It is the responsibility of the pilot to supervise the ground crew and ensure all items are completed prior to and after operating the aircraft.

Table 21: Flight Checklist

Preflight Inspection		Before Takeoff	
<b>AIRFRAME</b>		Propeller Area	CLEAR
Mission Payload	SECURED	Throttle Inhibit Switch	ON
All Receiver Connections	CHECKED	Motor Power	ARM PLUG
Motor and Avionics Batteries	CONNECTED	All Trims	SET
All Access Hatches	CLOSED	Flight Controls	CORRECT
Center of Gravity	WITHIN LIMITS	Throttle Inhibit Switch	OFF
Wings, Empennage, Ldg Gear	SECURE	Throttle Response Abv 50%	CHECK
Landing Gear Roll	SMOOTH		
<b>FLIGHT CONTROLS</b>		<b>After Landing</b>	
Propellers	TIGHTENED	Motor Power	DISARM PLUG
Radio Power	ON	Avionics/Receiver Power	OFF
Avionics/Receiver Power	ON	All Batteries	DISCONNECT
Flight Control Servo Linkages	CONNECTED	Radio Power	OFF
Touch Control Surfaces	DO NOT MOVE	Aircraft Structure	INSPECT

## 8 Performance Results

In order to validate design, a series of tests were conducted on the systems to verify performance.

### 8.1 Demonstrated System Performance

#### 8.1.1 Thrust Stand Results

Tests were carried out according to the routine devised under section 7.3.1. The first stage benchmarks the motor inventory to determine the top two motors with the greatest potential, by measuring the max thrust on a heavy-loading prop. As Figure 44 shows, the T-Motor AT3530 580KV and the iFlight XING X4214 660KV motor had approximately the same potential. Therefore, they were chosen as the two candidate motors for stage 2.

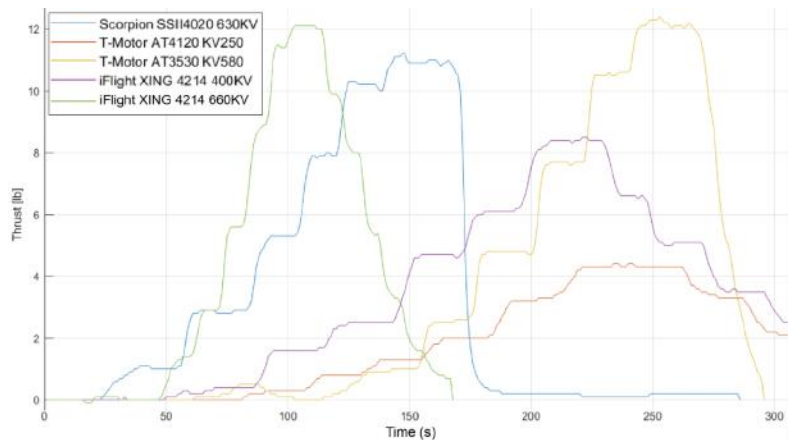


Figure 44: Motor Thrust Potential Evaluation

The stage 2 test consisted of a simulation load for the fastest configuration for Mission 2 using a 12 x 12 prop. Compared to the T-Motor AT3530, the iFlight X4214 used significantly more power for a marginal increase of thrust compared to that of the T-Motor AT3530, and thus was less efficient.

However, the team deduced that prop flow separation was present and decreased performance, as the static stand could not provide the 12 x 12 prop with sufficient incoming airflow. Additionally, the fact that drag was quadratically related to speed meant that the iFlight motor overcame more drag to achieve marginally more thrust, using more power in the process. Overall, since it was calculated to be within the energy limit of Mission 2 and weighed significantly less than the T-Motor AT3530, the iFlight XING X4214 was chosen to be installed on the Competition Aircraft.

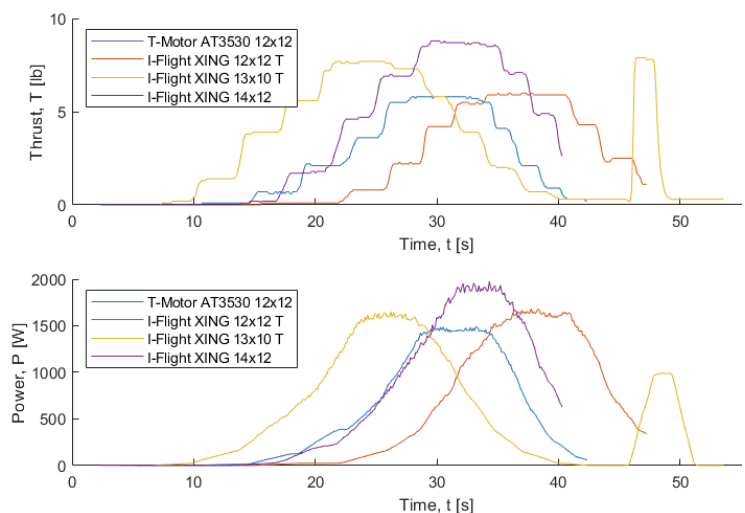


Figure 45: Thrust and Power versus Prop Choice

Stage 3 involved testing the final motor on different props to study motor behavior as well as prop correlation. A compiled plot is shown in Figure 45. The results from this contributed to prop optimizations for each mission.

### 8.1.2 Structural Testing

After performing the wing structure test on the XPS foam and carbon-Kevlar composite wing, the results were compared to the materials tested previously (21). As shown in Figure 46, a plot was created graphing the applied load versus the angle of deformation. The ideal material has the least angle of deformation for the greatest applied load (high stiffness). The carbon-Kevlar composite wing was capable of withstanding the highest ultimate load before fracturing at 23.8 pounds while also deforming the least out of all tested wings.

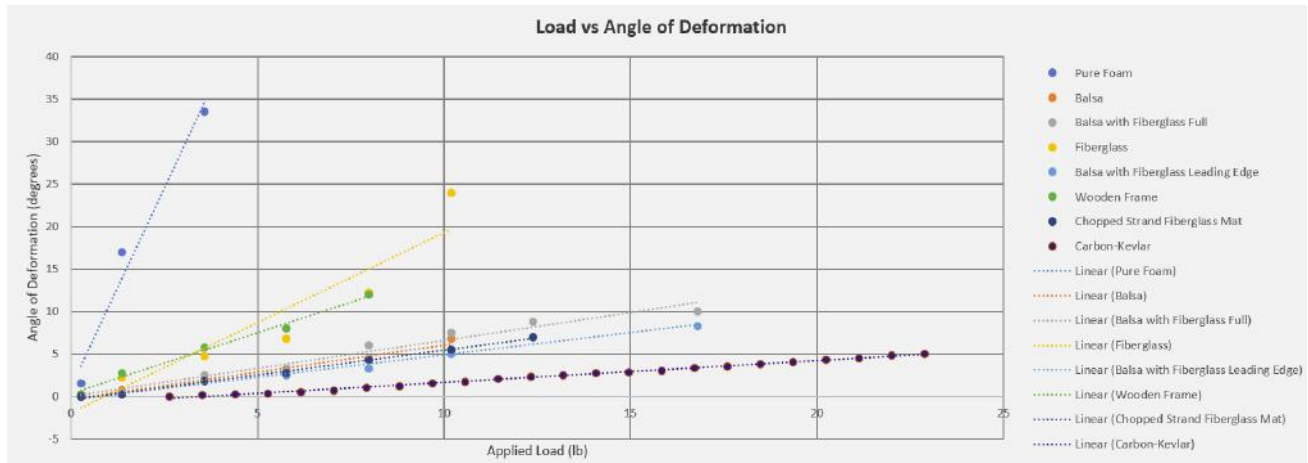


Figure 46: Graph of Wing Deformation vs Load

The maximum load that the airframe is expected to sustain during flight is 198 pounds (3g load, FOS 1.5), distributed across the front and rear wings. Figure 47 shows the fracture occurred during testing. As this test proved the wing can withstand a 23.8 pound point load at the tip of the wing, it can be stated that the wing can withstand this same load distributed across the wing, as the bending moment caused by the distributed load would be halved when compared to the point load.

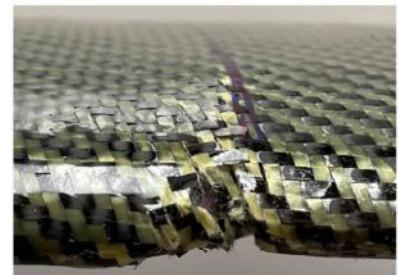


Figure 47: Wing Test Damage

Structure Type	Weight (lb)	Ultimate Load (lb)	Strength/Weight
Pure Foam	0.11	1.37	13
Balsa	0.21	10.19	48
Balsa with Fiberglass Leading Edge	0.28	16.80	60
Balsa with Fiberglass Full	0.30	16.80	56
Fiberglass	0.18	5.78	32
Chopped Strand Fiberglass Mat	0.44	12.39	28
Wooden Frame	0.24	4.67	20
Carbon-Kevlar	0.39	23.81	62

Table 22: Materials vs Strength/Weight

Additionally, the wing tested makes up only one quarter of the wing structure for the competition aircraft, as the *Dragonfly* has four wing sections of approximately this length. Furthermore, the structural I-beam running through the wing provides additional strength and stiffness. Table 22 verifies that the choice of carbon-Kevlar also increases the strength-to-weight ratio of the wing structure. Therefore, the Huskyworks team is confident that the selected composite can withstand the in-flight loads.

### 8.1.3 Sensor Stability

The flight demonstrations with the sensor tethered to a drone verified that the sensor was aerodynamically stable. As long as there was sufficient airspeed, the sensor remained in a fixed orientation on the yaw and pitch axes. The CG mounted tow cable helped stabilize the sensor along the roll axis at high and low speeds. The sensor made several close passes to the ground camera which collected video showing the sensor in stable flight, as seen in Figure 48. These flights validated the team's sensor body and fin design and demonstrated the sensor's stability in conditions similar to that of competition.



Figure 48: Sensor Flying on a Left-Hand Turn and a Straightaway

### 8.1.4 Sensor Deployment

The sensor was attached to the winch to verify that the weight of the sensor could be lifted with the servo motor. The geometry of the bomb-bay doors was verified in CAD and the actuators were tested to ensure that they could open and close the doors. During the second Competition Prototype flight test, the winch mechanism will be verified in flight.

### 8.1.5 Sensor Operation

The three stages of testing are detailed in section 7.3.5. After performing the first stage, the team determined that a common ground was not required for a PWM signal to travel from one Arduino to another. This meant only one connection to the plane is necessary for PWM input.

The second stage of testing was carried out to test the timing of the LEDs. When the code ran to perform this test, the LEDs turned on and off sequentially as intended. A one second delay was recorded between flashes and no LEDs burnt out from a current surge. The third stage of testing proved that the high-power LEDs turned on and off, alternating as intended. The use of relays protected the board from overheating. This test also showed that the three in-series 3.3-Ohm resistors were necessary. For the competition sensor, one 10-Ohm resistor will be used to conserve space. Figure 49 shows the high power LED light flashing.



Figure 49: High-Power LED

### 8.1.6 Sensor Container Drop-Test



Figure 50: Sensor and Container Before and After Drop Test

As shown in Figure 50, the sensor and container showed no visible signs of damage after the drop test. This proved to the team that, as anticipated, the container was strong enough. Moving forward the Huskyworks team will work to optimize the weight of the sensor box by applying relief cuts to the frame of the box. This will be tested iteratively until either the target weight is achieved or the box fails a drop test.

### 8.1.7 Aerodynamic Flight Test

The first flight with the Aerodynamic Prototype yielded a takeoff roll of approximately 30 feet from a grass field. Because the aircraft was anticipated to have strong nose-down tendencies based on aerodynamic simulations, the flaps on the front wing were partially deflected downward and the elevator trim was set above neutral to provide a nose-up moment. Upon takeoff in the first flight test, the aircraft began to climb rapidly, showing much less nose-down tendency than expected. When slightly rolled, a sideslip developed (Figure 51), causing the aircraft to lose speed and experience pitch oscillations until it stalled, rotated around its vertical axis, and impacted the ground. Based on pilot descriptions of aircraft handling and review of the flight footage taken via ground observation and quadcopter, the aircraft was determined to lack yaw stability. In order to compensate for this instability, the size of the vertical stabilizer was increased to better accommodate the size of the aircraft. The pilot also determined that the next flight should have no flaps and lower neutral elevator position to reduce the climb tendency.



Figure 51: Aerodynamic Prototype in Sideslip Condition

## 8.2 Demonstrated Aerodynamic Prototype Flight Performance

A second flight test was done with the Aerodynamic Prototype following recommended modifications from the first flight test. A larger vertical stabilizer and wheels were installed. Elevator trim was set to a lower neutral point and no flaps were used. For this flight, a longer ground roll and a shallower climb were executed to ensure that there was a margin of safety above stall and the aircraft's unknown characteristics were accounted for. The aircraft demonstrated pitch, roll, and yaw stability, requiring only slight elevator inputs to remain level and mostly nose-up, as shown by Figure 52. The elevator only used 20% input on the landing flare. Under the trim condition requiring slight elevator up input, the aircraft does not tend to stall itself if controls are released, which is ideal.

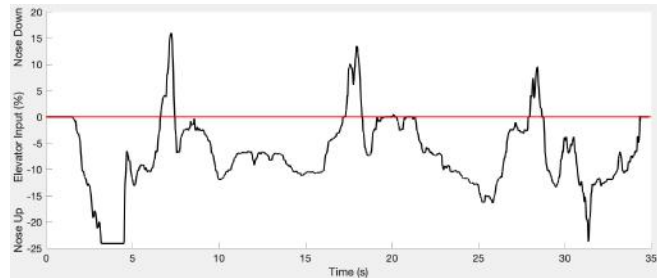


Figure 52: Elevator Control Stick Input

According to pitot tube data shown in Figure 53 the aircraft cruised between 60 and 70 ft/s (41-48 mph) at a throttle setting between 60 and 70%, touching down at 52 ft/s (35 mph). The plane touched down after a single 26 second lap was completed due to an audible motor surge that needed to be investigated. Despite this, flight stability was confirmed and the flight and landing were deemed successful. Two more flight tests will be completed with the Aerodynamic Prototype prior to flying the Competition Aircraft so that the pilot can get more comfortable with the characteristics of the aircraft.

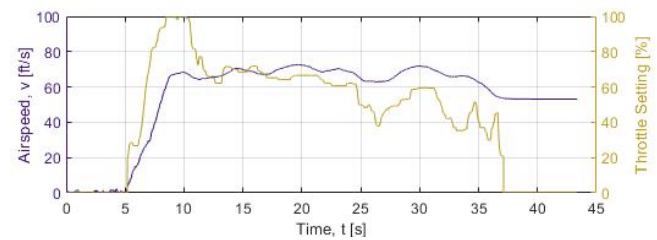


Figure 53: Throttle Setting vs Airspeed (Black-box Data)

At the time of this report, the Huskyworks team has only been able to test for Mission 1 parameters. However, the data that is available is promising. The team is within a 20% margin of the expected performance and due to the correlation between endurance and lap time/cruise velocity, it is likely that the predicted values can be met. The recorded data to date (February 19<sup>th</sup>) is shown in Table 23.

Table 23: Predicted versus Actual Flight Performance Parameters

	Parameter	Predicted Value	Proven Value	Percent Difference
Mission 1	Lap Time	35 seconds	42 seconds	-16.67%
	Cruise Velocity	85 feet per second	70 feet per second	-17.65%
	Endurance	12.0 minutes	13.4 minutes	10.45%
Mission 2	Lap Time	32 seconds	-----	n/a
	Number of Boxes	18	-----	n/a
	Endurance	2.1 minutes	-----	n/a
Mission 3	Lap Time	35 seconds	-----	n/a
	Endurance	12.0 minutes	-----	n/a
Ground Mission	Completion	120 seconds	-----	n/a

## References

- [1] Raymer, D., *Aircraft Design: A Conceptual Approach*, American Institute of Aeronautics and Astronautics, Inc., 6th ed., 2018.
- [2] Nicolai, L. and Carichner, G., *Fundamentals of Aircraft and Airship Design*, Vol. 1, American Institute of Aeronautics and Astronautics, Inc., 2010.
- [3] Anderson, J., *Introduction to Flight*, McGraw-Hill Education, New York, NY, 8th ed., 2016.
- [4] Kenji Tadakuma, Y. T. and Aso, S., "Effect of Fuselage Cross Section on Aerodynamic Characteristics of Reusable Launch Vehicles," *Open Journal of Fluid Dynamics*, , No. 6, Sep 2016, pp. 222–233.
- [5] Diehl, W. S., *Engineering Aerodynamics*, The Ronald Press Company., 1928.
- [6] *AT3530 Long Shaft*, T-Motor, 2020.
- [7] *XING X4214 2-8S X-CLASS FPV NextGen Motor*, iFlight Quads, 2020.
- [8] *SII-4020-630 Motor Propeller Data*, Scorpion Motors, 2020.
- [9] *Airfoil Tools*, 2020.
- [10] Drela, M., *XFOIL 6.99*, Massachusetts Institute of Technology, 2020.
- [11] Drela, M., *AVL*, Massachusetts Institute of Technology, 2020.
- [12] *SOLIDWORKS 2021*, Dassault Systemes, 2020.
- [13] *ANSYS Student*, Ansys Inc., 2020.
- [14] *OpenVSP*, National Aeronautics and Space Administration, 2020.
- [15] Niskanen, S., "OpenRocket Simulator," 2020.
- [16] *Drag of Nose Cones*, Apogee Components, 2013.
- [17] *Rocket Stability*, National Aeronautics and Space Administration, 2020.
- [18] *Flying Qualities of Piloted Aircraft*, June 1995, MIL-STD-1797A.
- [19] *Carbon Fiber I-Beam Specifications*, Dragon Plate.
- [20] Zhu, J. and Zhang, W., "A review of topology optimization for additive manufacturing: Status and challenges," *Chinese Journal of Aeronautics*, Vol. 34, 2010.
- [21] *Summer Composites Report*, DBF at the University of Washington, 2020.